



This is a repository copy of *OSL-thermochronometry of feldspar from the KTB borehole, Germany.*

White Rose Research Online URL for this paper:
<http://eprints.whiterose.ac.uk/109132/>

Version: Supplemental Material

Article:

Guralnik, B., Jain, M., Herman, F. et al. (9 more authors) (2015) OSL-thermochronometry of feldspar from the KTB borehole, Germany. *Earth and Planetary Science Letters*, 423. pp. 232-243. ISSN 0012-821X

<https://doi.org/10.1016/j.epsl.2015.04.032>

Reuse

Unless indicated otherwise, fulltext items are protected by copyright with all rights reserved. The copyright exception in section 29 of the Copyright, Designs and Patents Act 1988 allows the making of a single copy solely for the purpose of non-commercial research or private study within the limits of fair dealing. The publisher or other rights-holder may allow further reproduction and re-use of this version - refer to the White Rose Research Online record for this item. Where records identify the publisher as the copyright holder, users can verify any specific terms of use on the publisher's website.

Takedown

If you consider content in White Rose Research Online to be in breach of UK law, please notify us by emailing eprints@whiterose.ac.uk including the URL of the record and the reason for the withdrawal request.



eprints@whiterose.ac.uk
<https://eprints.whiterose.ac.uk/>

Supplementary material for:

OSL-thermochronometry of feldspar from the KTB borehole, Germany

Benny Guralnik ^{a,b,c,*}, Mayank Jain ^b, Frédéric Herman ^d, Christina Ankjærgaard ^c,
Andrew S. Murray ^e, Pierre G. Valla ^d, Frank Preusser ^f, Georgina E. King ^d, Reuven Chen ^g,
Sally E. Lowick ^h, Myungho Kook ^b, Edward J. Rhodes ^{i,j}

^a Department of Earth Sciences, ETH, 8092 Zürich, Switzerland

^b Centre for Nuclear Technologies, DTU–Risø, Frederiksborgvej 399, Building 201, 4000 Roskilde, Denmark

^c Soil Geography and Landscape group and the Netherlands Centre for Luminescence Dating, Wageningen University, Droevendaalsesteeg 3, 6708PB Wageningen, The Netherlands

^d Institute of Earth Surface Dynamics, University of Lausanne, Geopolis, 1015 Lausanne, Switzerland

^e Nordic Laboratory for Luminescence Dating, Aarhus University, Frederiksborgvej 399, Building 201, 4000 Roskilde, Denmark

^f Institute of Earth and Environmental Sciences – Geology, University of Freiburg, Albertstr. 23b, 72104 Freiburg, Germany

^g Raymond and Beverly Sackler School of Physics and Astronomy, Tel Aviv University, Tel Aviv 69978, Israel

^h Institute of Geological Sciences, University of Bern, Baltzerstrasse 1+3, 3012 Bern, Switzerland

ⁱ Department of Earth, Planetary, and Space Sciences, UCLA, Los Angeles, CA 90095-1567, USA

^j Department of Geography, University of Sheffield, Sheffield S10 2TN, UK

Published in *Earth and Planetary Science Letters* (2015), <http://dx.doi.org/10.1016/j.epsl.2015.04.032>

Contents:

Part I – Labwork and Dosimetry

S1. Laboratory procedures for extraction of feldspar (and quartz) from bedrock	2
S2. Whole-rock geochemistry (major elements)	3
S3. Whole-rock geochemistry (trace elements)	4
S4. Mineralogical composition of aliquots	5
S5. Dose rate scenarios	6

Part II – Luminescence

S6. Characterisation of electron trapping and detrapping kinetics	7
S7. Validation of the dosimetric protocol	19

Part III – Interpretation

S8. Screening of field-saturated samples	20
S9. Sensitivity of the inversion to natural dose rate	21
S10. Multivariate statistics on model parameters and observations	22

Part I – Labwork and Dosimetry

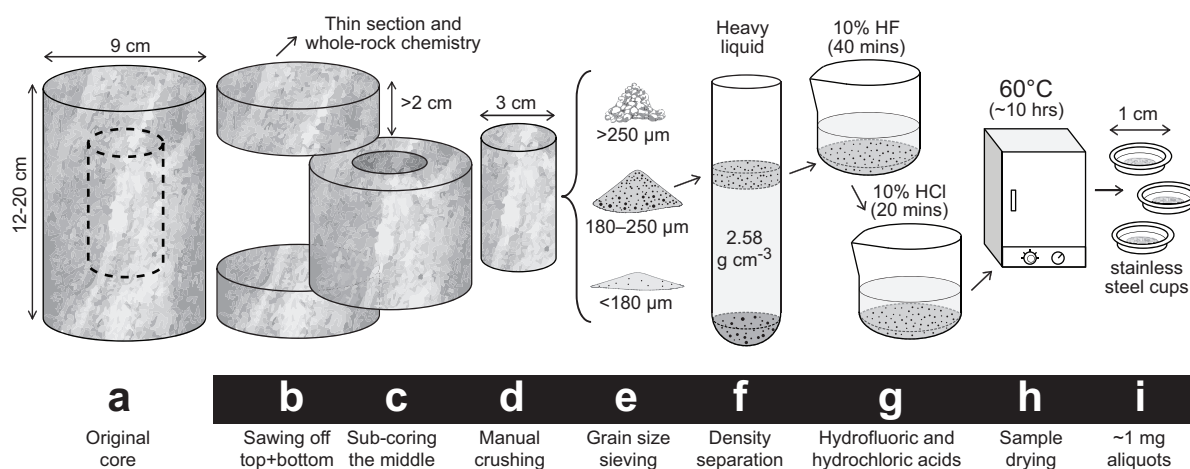


Figure S1. Laboratory procedures for extraction of feldspar (and quartz) from bedrock.

Table S1. Laboratory procedures for extraction feldspar (and quartz) from bedrock.

Step	Conditions	Action
a	Daylight	Acquisition of core samples, with emphasis on avoiding brittle or fractured rocks, or highly inhomogeneous rock textures (e.g. large leucocratic veins that could accelerate the optical bleaching of the minerals within).
b	Dark room	The top and bottom sides of the core are slowly sliced off, using a large diamond saw under a continuous and abundant supply of cooling water. One of these slices (~100 g) is milled and sent to chemical analyses; the other is cut to give a geological thin section.
c	Dark room	The optically-unbleached middle part of the core is slowly extracted, using a smaller-diameter diamond core drill under a continuous and abundant supply of cooling water.
d	Dark room	The optically-unbleached sub-core is thoroughly dried, and crushed by a geological sledge hammer to a target size fraction of 180 – 250 μm .
e	Dark room	The crushed material is manually sieved to collect the 180 – 250 μm size fraction. The larger fraction may be re-crushed; the smaller fraction is stored away.
f	Dark room	The 180 – 250 μm size fraction is subjected to two density separations in Lithium Sodium Tungstate (LST). After an initial step ($\rho = 2.70 \text{ g cm}^{-3}$), intended to rid of heavy minerals, the floating $\rho < 2.70 \text{ g cm}^{-3}$ density fraction is further immersed in $\rho = 2.58 \text{ g cm}^{-3}$. After sufficient separation, the $\rho < 2.58 \text{ g cm}^{-3}$ (feldspar) and the $2.58 < \rho < 2.70 \text{ g cm}^{-3}$ (quartz) density fractions are collected and thoroughly rinsed in water.
g	Dark room	To dissolve the outer rims of grains (affected by external alpha radiation), the $\rho < 2.62 \text{ g cm}^{-3}$ density fraction (feldspar) is etched in a 10% (vol.) HF solution for 40 minutes, rinsed in distilled water, and subsequently treated with a 10% (vol.) HCl solution for 20 minutes to dissolve fluorides. The $\rho > 2.62 \text{ g cm}^{-3}$ density fraction (quartz) is etched in a 48% (vol.) HF solution for 60 minutes, rinsed in distilled water, and subsequently treated with a 10% (vol.) HCl solution for 40 minutes.
h	Dark room	A thoroughly rinsed sample is dried overnight (~10 hours) in a 60 °C light-tight oven.
i	Dark room	The dried sample is used to prepare ~1 mg aliquots, each consisting of a monolayer of grains evenly distributed over the surface (4 – 6 mm in diameter) of a silicone-sprayed stainless-steel cup, which is then loaded into a Risø TL/OSL reader.

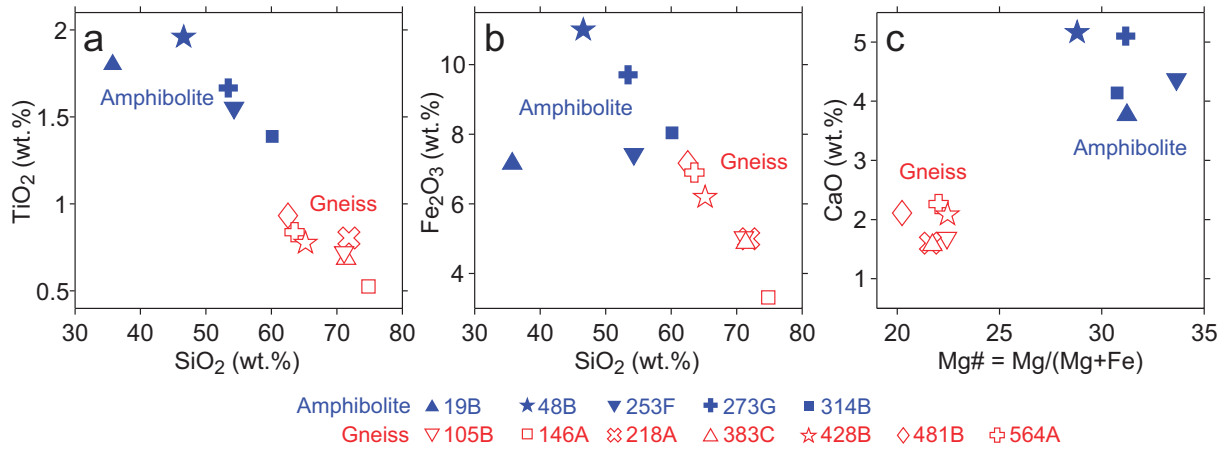


Figure S2. Whole-rock geochemistry (major elements). Representative oxide or elemental ratios (a-c) for KTB amphibolites (blue) and paragneisses (red) suggest silica-poor protoliths for the amphibolites (mid-ocean ridge basalts), and silica-rich protoliths for the paragneisses (young terrigenous sediments).

Table S2. Whole-rock geochemistry (major elements).

Sample ID	Depth (km)	0.146 19B	0.334 48B	0.566 105B	0.726 146A	0.911 218A	1.175 253F	1.300 273G	1.499 314B	1.730 383C	1.892 428B	2.097 481B	2.329 564A
SiO ₂ (wt.%)		35.76	46.60	71.10	74.84	71.84	54.31	53.42	60.13	71.40	65.21	62.55	63.54
TiO ₂		1.80	1.96	0.72	0.53	0.80	1.55	1.67	1.39	0.69	0.77	0.93	0.84
Al ₂ O ₃		12.23	14.71	13.41	12.76	13.34	17.40	16.87	15.00	13.90	16.95	17.65	16.43
Fe ₂ O ₃ (Total)		7.16	11.00	5.04	3.31	5.00	7.43	9.71	8.04	4.88	6.19	7.17	6.90
MnO		0.21	0.17	0.10	0.05	0.07	0.13	0.19	0.13	0.09	0.09	0.15	0.10
MgO		3.77	5.16	1.69	0.89	1.60	4.37	5.10	4.14	1.57	2.08	2.11	2.26
CaO		18.18	12.87	1.44	1.54	1.29	7.71	7.27	6.68	1.17	0.83	1.04	1.39
Na ₂ O		3.63	3.07	2.79	3.88	2.84	4.19	3.96	3.81	3.02	2.65	2.95	3.20
K₂O		1.08	0.46	1.80	1.49	2.21	1.50	0.58	0.53	2.07	2.92	2.82	2.87
P ₂ O ₅		0.42	0.27	0.10	0.12	0.11	0.23	0.21	0.18	0.12	0.10	0.14	0.14
Loss on ignition		15.82	3.34	2.52	1.19	1.25	1.46	0.94	0.75	1.75	2.18	2.26	1.90
Total		100.1	99.6	100.7	100.6	100.3	100.3	99.9	100.8	100.7	100.0	99.8	99.6

Major oxides (in wt.%) were analyzed at Activation Laboratories Ltd. (Ancaster, Ontario) by inductively coupled plasma (ICP) optical emission spectrometry (OES), and mass spectrometry (MS). All oxides were determined on a Varian Vista 735-ES ICP-OES. Estimated instrumental precision is 1.3% for K₂O (marked in bold, used for natural dose-rate estimation), and 2.9% (average for all oxides). Conversion of K₂O (reported here) into K (reported in Table 1 in the main text) is through multiplication by a factor of 0.8301.

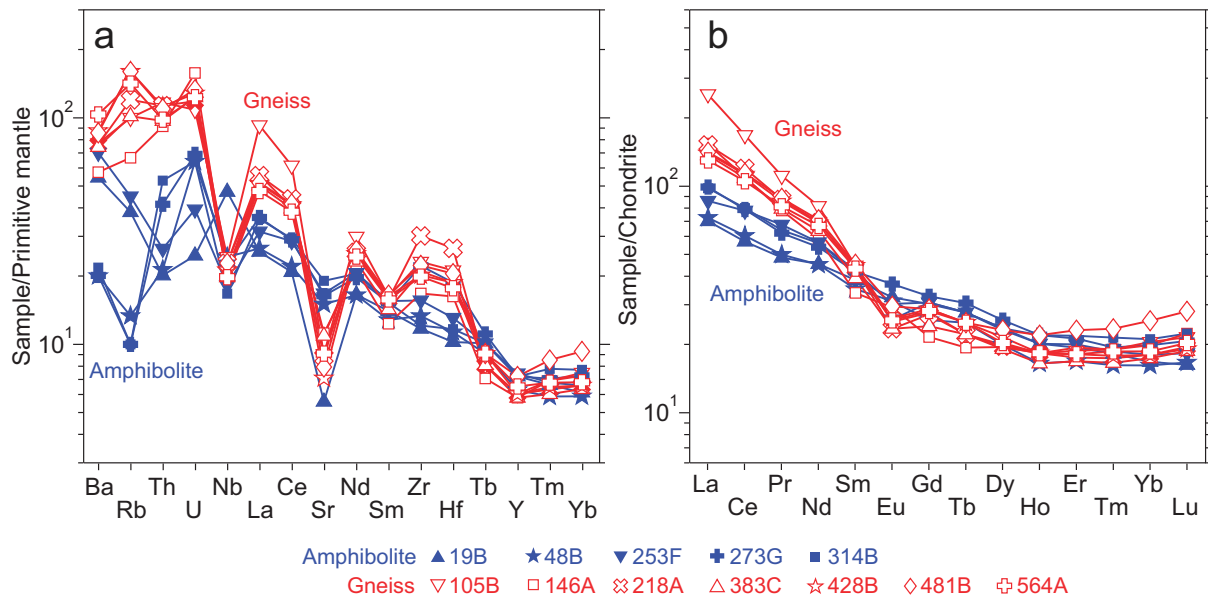


Figure S3. Whole-rock geochemistry (trace elements). Trace elements of KTB amphibolites (blue) and paragneisses (red) are shown using standard geochemical normalization to primitive mantle (a) and chondrite (b), exhibiting a lower-crust (amphibolite) and upper-crust (paragneiss) trace-element fractionation patterns, respectively.

Table S3. Whole-rock geochemistry (trace elements).

Sample	Depth (km) ID	0.146 19B	0.334 48B	0.566 105B	0.726 146A	0.911 218A	1.175 253F	1.300 273G	1.499 314B	1.730 383C	1.892 428B	2.097 481B	2.329 564A
Sc (ppm)	14	28	14	9	13	25	25	23	13	16	23	18	
V	128	262	105	70	102	181	180	182	93	127	162	144	
Cr	90	180	80	770	80	80	160	140	70	90	120	90	
Co	18	34	14	17	14	22	36	30	14	18	19	19	
Ni	50	80	50	370	50	< 20	90	60	50	60	70	60	
Cu	40	50	20	40	30	30	60	40	30	30	50	40	
Zn	70	100	80	80	90	80	140	90	90	110	110	120	
Rb	23	8	60	40	72	27	6	6	61	96	96	85	
Sr	111	299	180	223	175	334	326	379	217	141	158	181	
Y	31	27	26	25	26	32	31	31	25	26	31	28	
Zr	123	140	243	176	316	164	233	127	220	212	234	209	
Nb	31	16	16	13	15	12	15	11	13	14	15	13	
Cs	0.6	< 0.5	3.0	1.4	3.0	1.2	0.9	0.6	2.5	4.1	2.8	3.8	
Ba	359	132	509	380	503	463	133	144	491	578	566	683	
La	16.6	17.2	60.1	36.3	36.0	20.4	23.5	23.2	32.5	33.1	33.5	30.8	
Ce	34.9	37.0	103.0	67.2	73.5	47.8	48.4	49.1	66.7	69.1	69.9	64.5	
Pr	4.5	4.6	10.3	7.2	8.1	6.3	5.8	6.0	7.4	8.0	8.2	7.6	
Nd	20.7	20.6	37.3	26.7	31.8	25.8	24.6	25.6	29.0	31.4	32.5	30.5	
Sm	5.7	5.2	6.6	5.0	6.4	6.3	6.2	6.2	5.8	6.6	6.7	6.4	
Eu	1.8	1.8	1.4	1.6	1.3	1.5	2.1	1.7	1.3	1.5	1.7	1.4	
Gd	6.0	5.1	5.5	4.3	5.4	6.1	6.5	6.1	4.8	5.7	5.7	5.6	
Tb	1.0	0.9	0.8	0.7	0.8	1.0	1.1	1.0	0.8	0.9	0.9	0.9	
Dy	5.7	4.9	4.9	4.8	4.8	5.8	6.3	5.8	4.7	5.3	5.7	5.0	
Ho	1.1	0.9	1.0	1.0	1.0	1.1	1.2	1.2	0.9	1.0	1.2	1.0	
Er	3.1	2.7	3.0	3.1	2.8	3.2	3.4	3.5	2.7	2.9	3.7	2.9	
Tm	0.5	0.4	0.5	0.5	0.4	0.5	0.5	0.5	0.4	0.4	0.6	0.5	
Yb	2.7	2.6	3.3	3.2	2.9	2.9	3.2	3.4	2.8	2.9	4.1	3.0	
Lu	0.4	0.4	0.5	0.6	0.5	0.5	0.5	0.6	0.5	0.5	0.7	0.5	
Hf	2.9	3.2	6.0	4.6	7.5	3.7	5.3	3.3	5.3	5.3	5.8	5.0	
Pb	< 5	< 5	13	20	12	6	< 5	< 5	13	18	18	14	
Th	1.6	1.7	9.3	7.3	9.0	2.1	3.3	4.2	7.7	8.9	8.7	7.8	
U	0.5	1.3	2.2	3.2	2.4	0.8	1.4	1.3	2.5	2.6	2.7	2.5	

Trace elements (in ppm.) were analyzed at Activation Laboratories Ltd. (Ancaster, Ontario) by inductively coupled plasma (ICP) optical emission spectrometry (OES), and mass spectrometry (MS). The elements Sc, V, Sr, Y, Zr, Ba were determined on a Varian Vista 735-ES ICP-OES; all other elements were measured on a Perkin Elmer Sciex ELAN 6100/9000 ICP-MS. Estimated instrumental precision is 3.9% for U and Th (marked in bold, used for natural dose-rate estimation), and 3.7% (average for all trace elements).

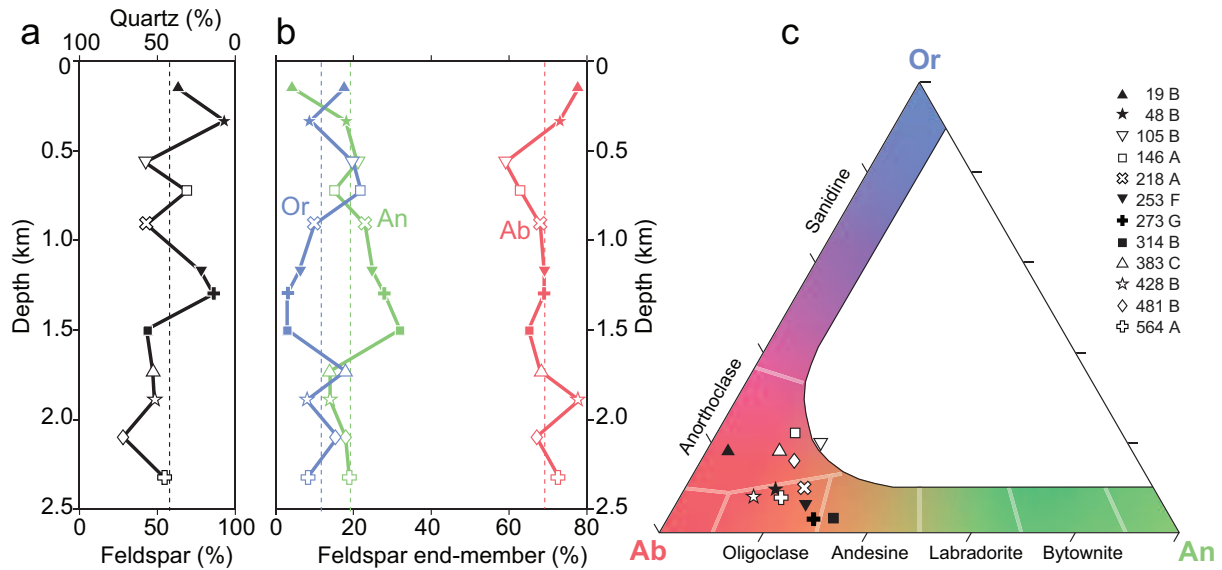


Figure S4. Mineralogical composition of aliquots. (a-b) Aliquot composition vs. sample depth (means are represented by dashed lines), as measured by a prototype X-Ray Fluorescence (XRF) attachment to Risø TL/OSL reader. (c) Feldspar composition from (b) plotted on a ternary feldspar diagram.

Table S4. Mineralogical composition of aliquots and estimation of potassium content in feldspar.

Sample	Measurements				Calculated values			
	Depth (km)	ID	Aliquot mineralogy determined by XRF				Or/(Ab+An+Or)	K _{int}
			Qz (wt. %)	Ab (wt. %)	An (wt. %)	Or (wt. %)	(wt.%)	(wt.%)
0.146	19B		38.0 ± 1.9	48.5 ± 2.0	2.6 ± 0.1	10.9 ± 0.2	17.6	2.46
0.334	48B		6.5 ± 1.3	67.9 ± 1.6	16.9 ± 0.1	8.7 ± 0.1	9.3	1.30
0.566	105B		57.5 ± 15.0	25.1 ± 16.7	8.8 ± 0.9	8.6 ± 0.9	20.2	2.82
0.726	146A		30.7 ± 18.2	43.6 ± 21.4	10.5 ± 1.3	15.2 ± 2.0	22.0	3.08
0.911	218A		56.6 ± 3.0	29.3 ± 3.4	9.8 ± 0.2	4.2 ± 0.2	9.7	1.36
1.175	253F		21.9 ± 2.6	53.8 ± 3.2	19.8 ± 0.3	4.6 ± 0.3	5.9	0.82
1.300	273G		14.1 ± 6.0	59.1 ± 8.0	24.2 ± 1.4	2.6 ± 1.0	3.0	0.42
1.499	314B		57.4 ± 2.2	27.9 ± 2.6	13.6 ± 0.3	1.2 ± 0.2	2.8	0.39
1.730	383C		52.8 ± 3.2	31.9 ± 3.0	6.8 ± 0.2	8.6 ± 0.3	18.1	2.54
1.892	428B		51.5 ± 2.1	37.8 ± 2.4	6.7 ± 0.2	4.0 ± 0.2	8.2	1.14
2.097	481B		72.5 ± 8.5	18.4 ± 8.5	4.9 ± 0.5	4.3 ± 0.3	15.6	2.18
2.329	564A		45.0 ± 2.7	40.2 ± 3.3	10.7 ± 0.3	4.2 ± 0.3	7.7	1.08

Mineral fractions in a luminescence aliquot, as determined by the Risø XRF attachment (see text). Qz – quartz, Ab – albite, An – anorthite, Or – orthoclase. On average, aliquots consist of ~42% pure quartz and ~58% feldspar (Ab₆₉An₁₉Or₁₂). The latter composition, characteristic of anorthoclase-oligoclase, could in fact represent a mix of pure end-members. The fractional weight of the orthoclase end-member (fifth column, average uncertainty of ~15%) is further multiplied by the stoichiometric 14% wt.% K in orthoclase to yield an estimate of the total K content in feldspar.

Homogeneous distribution of internal potassium (K_{int}) within a single feldspar phase (anorthoclase or oligoclase). IRSL₅₀ originates from entire crystal.

Non-homogeneous distribution of internal potassium (K_{int}) across adjacent feldspar phases. IRSL₅₀ originates solely from K-feldspar

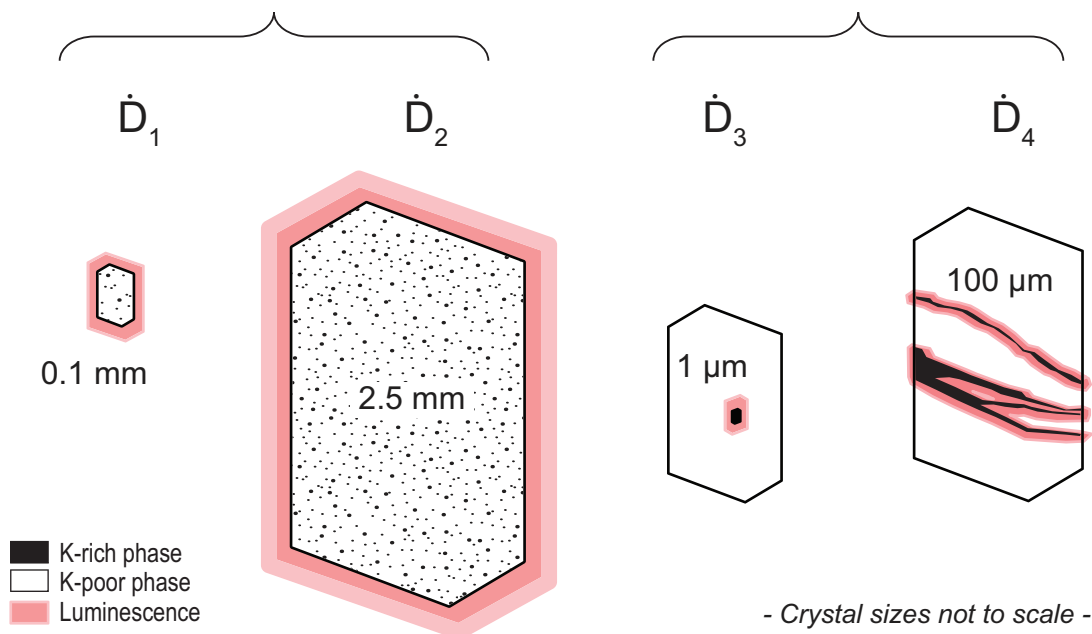


Figure S5. Dose rate scenarios. Scenarios \dot{D}_1 and \dot{D}_2 involve two different crystal sizes of a K-poor feldspar phase, where the internal potassium (black dots) is homogeneously distributed within the entire grain, with luminescence arising from the entire grain as well. Scenarios \dot{D}_3 and \dot{D}_4 involve two different crystal sizes of a multiphase feldspar mixture, in which luminescence arises only from the K-feldspar phase(s) corresponding to high internal potassium (black areas). The actual KTB rocks are dominated by scenarios \dot{D}_1 and \dot{D}_2 , but may contain rare instances of \dot{D}_3 and \dot{D}_4 .

Table S5. Dose rate scenarios.

Sample		Measurements				Model dose rates ^c				
		Radionuclides			Feldspar ^b	Anorthoclase / Oligoclase		Pure orthoclase		Average
Depth (km)	ID	U (ppm)	Th (ppm)	K (wt.%)		0.1 mm \dot{D}_1 (Gy ka ⁻¹)	2.5 mm \dot{D}_2 (Gy ka ⁻¹)	1 μm \dot{D}_3 (Gy ka ⁻¹)	100 μm \dot{D}_4 (Gy ka ⁻¹)	
0.146	19B	0.5	1.6	0.90	2.46	1.19 ± 0.02	2.17 ± 0.28	1.17 ± 0.02	1.47 ± 0.02	1.50
0.334	48B	1.3	1.7	0.38	1.30	0.85 ± 0.01	1.27 ± 0.15	0.85 ± 0.01	1.16 ± 0.02	1.03
0.566	105B	2.2	9.3	1.49	2.82	2.74 ± 0.04	3.14 ± 0.33	2.79 ± 0.04	3.01 ± 0.04	2.92
0.726	146A	3.2	7.3	1.24	3.08	2.59 ± 0.04	3.26 ± 0.36	2.63 ± 0.04	2.86 ± 0.04	2.84
0.911	218A	2.4	9.0	1.83	1.36	3.07 ± 0.05	2.20 ± 0.16	3.17 ± 0.05	3.38 ± 0.05	2.96
1.175	253F	0.8	2.1	1.25	0.82	1.60 ± 0.03	1.16 ± 0.10	1.64 ± 0.03	1.93 ± 0.03	1.58
1.300	273G	1.4	3.3	0.48	0.42	1.06 ± 0.02	0.75 ± 0.05	1.10 ± 0.02	1.39 ± 0.02	1.07
1.499	314B	1.3	4.2	0.44	0.39	1.05 ± 0.02	0.74 ± 0.05	1.10 ± 0.02	1.39 ± 0.02	1.07
1.730	383C	2.5	7.7	1.72	2.54	2.92 ± 0.05	2.97 ± 0.29	2.98 ± 0.04	3.20 ± 0.05	3.02
1.892	428B	2.6	8.9	2.42	1.14	3.69 ± 0.06	2.25 ± 0.14	3.82 ± 0.06	4.01 ± 0.06	3.44
2.097	481B	2.7	8.7	2.34	2.18	3.65 ± 0.06	2.97 ± 0.25	3.75 ± 0.06	3.93 ± 0.06	3.57
2.329	564A	2.5	7.8	2.38	1.08	3.55 ± 0.06	2.13 ± 0.13	3.67 ± 0.06	3.86 ± 0.06	3.30

^a Whole-rock concentrations of the radioactive elements (U, Th and K=0.8301×K₂O) are repeated/recalculated from Tables S2-S3. For external dose-rate calculation, we assume uncertainties of 1.3% for K₂O, and 3.9% for U and Th (corresponding to the precision of ICP).

^b Feldspar concentrations of internal K_{int} in feldspar is repeated from Table S4. For internal dose-rate calculation, we assume uncertainties of 15% (average precision of the XRF data; Table S4).

^c Dose rates corresponding to each particular scenario (numbered 1-4 accordingly) were calculated using the radionuclide-specific dose rates, beta self-dose parameters, and moisture correction factors from Guérin et al. (2012). Moisture content was estimated at 2±2% for all samples; any contribution of alpha and/or cosmic radiation was neglected. The last column (in bold) is an arithmetic mean of dose rates in the four preceding columns.

Part II – Luminescence

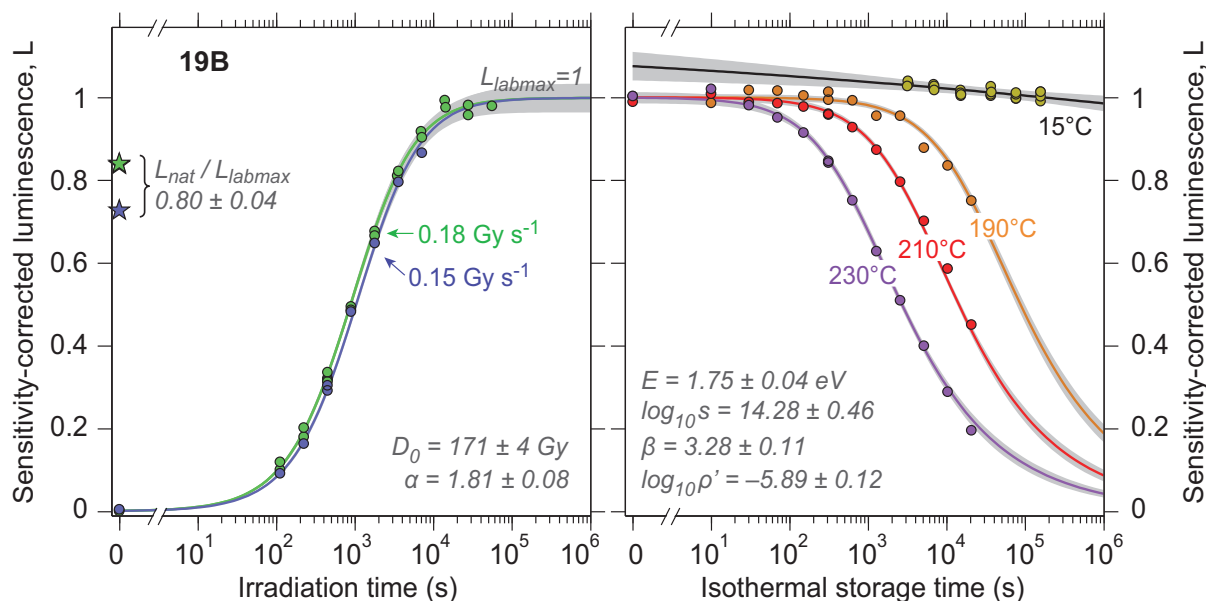


Figure S6-1. Characterisation of electron trapping and detrapping kinetics (19B). Radiation-induced growth (circles, left panel) and isothermal decay (circles, right panel) of sample 19B. Stars in left panel denote natural luminescence levels. Note that the y-axis of the shown data and its simultaneous best-fits are arbitrarily rescaled for convenience of presentation (laboratory saturation at $L=1$ in left panel; initial luminescence of $L=1$ in right panel).

Table S6-1. Characterisation of electron trapping and detrapping kinetics (19B).

19B																
T (°C)	15	t (ks)	Nat	0.111	0.222	0.444	0.889	1.778	3.472	6.944	13.889	27.778	55.556	0.000	0.444	27.778
\dot{D} (Gy/s)	0.18	Lx/Tx	3.903	0.468	0.839	1.478	2.306	3.154	3.783	4.277	4.630	4.574	4.567	0.015	1.499	4.462
T (°C)	15	t (ks)	Nat	0.111	0.222	0.444	0.889	1.778	3.556	7.111	14.222	0.000	0.444			
\dot{D} (Gy/s)	0.18	Lx/Tx	3.695	0.525	0.889	1.379	2.141	2.929	3.616	3.975	4.293	0.005	1.481			
T (°C)	15	t (ks)	Nat	0.111	0.222	0.444	0.889	1.778	3.556	7.111	0.000	0.444				
\dot{D} (Gy/s)	0.153	Lx/Tx	3.762	0.473	0.846	1.575	2.496	3.359	4.124	4.486	0.027	1.513				
T (°C)	230	t (ks)	0.000	0.010	0.030	0.070	0.150	0.310	0.630	1.270	2.550	5.110	10.230	20.470	0.310	
\dot{D} (Gy/s)	0	Lx/Tx	0.885	0.899	0.865	0.839	0.807	0.742	0.663	0.553	0.449	0.352	0.254	0.172	0.746	
T (°C)	210	t (ks)	0.000	0.010	0.030	0.070	0.150	0.310	0.630	1.270	2.550	5.110	10.230	20.470	0.310	
\dot{D} (Gy/s)	0	Lx/Tx	0.942	0.960	0.941	0.938	0.930	0.914	0.883	0.831	0.757	0.667	0.557	0.429	0.912	
T (°C)	190	t (ks)	0.000	0.010	0.030	0.070	0.150	0.310	0.630	1.270	2.550	5.110	10.230	20.470	0.310	
\dot{D} (Gy/s)	0	Lx/Tx	0.970	0.954	0.985	0.983	0.972	0.962	0.960	0.924	0.925	0.850	0.808	0.726	0.981	
T (°C)	15	t (ks)	0.354	4.440	3.247	6.742	14.932	36.427	75.917	156.33						
\dot{D} (Gy/s)	0	Lx/Tx	0.042	0.043	0.925	0.918	0.912	0.920	0.894	0.888						
T (°C)	15	t (ks)	0.352	4.377	3.215	6.829	15.019	36.513	76.004	156.42						
\dot{D} (Gy/s)	0	Lx/Tx	0.082	0.062	0.985	0.985	0.965	0.958	0.952	0.968						
T (°C)	15	t (ks)	0.354	4.344	3.181	6.855	15.103	36.598	76.088	156.50						
\dot{D} (Gy/s)	0	Lx/Tx	1.022	1.041	1.048	1.036	1.013	1.016	1.016	1.010						
T (°C)	15	t (ks)	0.352	4.344	3.149	6.856	15.190	36.684	76.174	156.59						
\dot{D} (Gy/s)	0	Lx/Tx	0.804	0.887	0.905	0.896	0.886	0.892	0.891	0.893						

Observations in grey strikethrough are deemed as laboratory artefacts (unexplained signal growth rather than its athermal decay) and hence rejected.

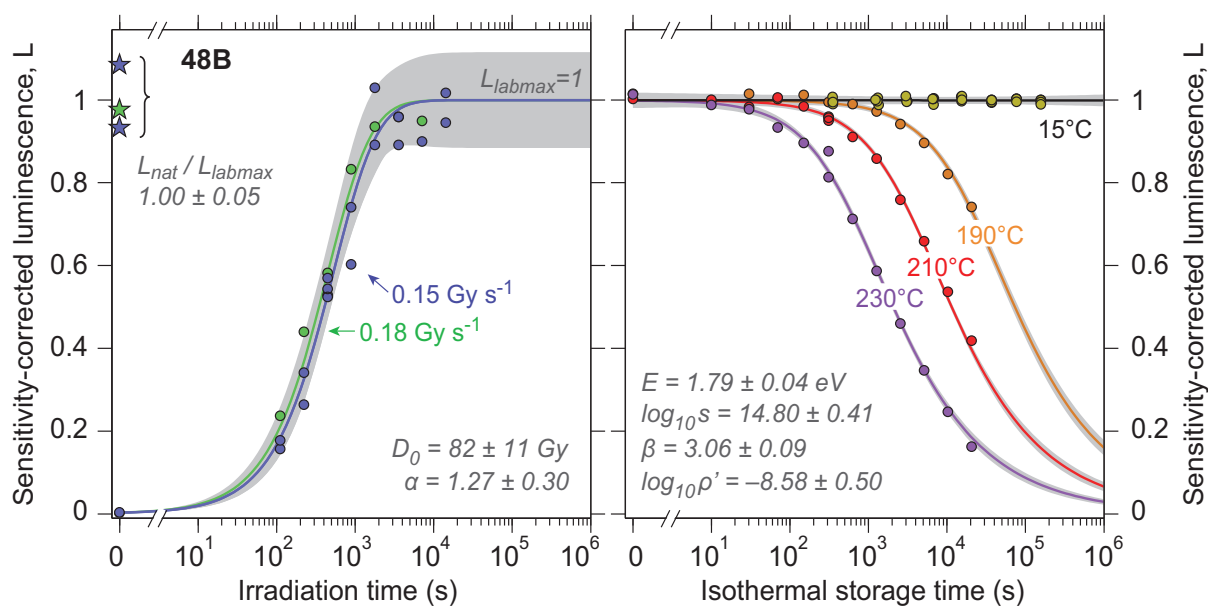


Figure S6-2. Characterisation of electron trapping and detrapping kinetics (48B). Radiation-induced growth (circles, left panel) and isothermal decay (circles, right panel) of sample 48B. Stars in left panel denote natural luminescence levels. Note that the y-axis of the shown data and its simultaneous best-fits are arbitrarily rescaled for convenience of presentation (laboratory saturation at $L=1$ in left panel; initial luminescence of $L=1$ in right panel).

Table S6-2. Characterisation of electron trapping and detrapping kinetics (48B).

48B															
$T (^{\circ}\text{C})$	15	$t(\text{ks})$	Nat	0.111	0.222	0.444	0.889	1.778	3.556	7.111					
$\dot{D}(\text{Gy/s})$	0.18	Lx/Tx	1.786	0.432	0.804	1.064	1.523	1.712	1.755	1.737					
$T (^{\circ}\text{C})$	15	$t(\text{ks})$	Nat	0.111	0.222	0.444	0.889	1.778	3.556	7.111	14.222	0.000	0.444		
$\dot{D}(\text{Gy/s})$	0.153	Lx/Tx	2.051	0.343	0.749	1.162	1.323	1.959	1.959	2.702	2.078	0.003	1.252		
$T (^{\circ}\text{C})$	15	$t(\text{ks})$	Nat	0.111	0.222	0.444	0.889	1.778	3.556	7.111	14.222	0.000	0.444		
$\dot{D}(\text{Gy/s})$	0.153	Lx/Tx	2.483	0.405	0.601	1.242	1.694	2.355	2.195	2.057	2.327	0.005	1.199		
$T (^{\circ}\text{C})$	230	$t(\text{ks})$	0.000	0.010	0.030	0.070	0.150	0.310	0.630	1.270	2.550	5.110	10.230	20.470	0.310
$\dot{D}(\text{Gy/s})$	0	Lx/Tx	0.865	0.844	0.835	0.797	0.765	0.695	0.608	0.501	0.393	0.296	0.210	0.138	0.748
$T (^{\circ}\text{C})$	210	$t(\text{ks})$	0.000	0.010	0.030	0.070	0.150	0.310	0.630	1.270	2.550	5.110	10.230	20.470	0.310
$\dot{D}(\text{Gy/s})$	0	Lx/Tx	0.951	0.948	0.932	0.954	0.934	0.901	0.863	0.813	0.719	0.624	0.508	0.396	0.907
$T (^{\circ}\text{C})$	190	$t(\text{ks})$	0.000	0.010	0.030	0.070	0.150	0.310	0.630	1.270	2.550	5.110	10.230	20.470	0.310
$\dot{D}(\text{Gy/s})$	0	Lx/Tx	0.992	0.976	0.992	0.979	0.989	0.972	0.968	0.950	0.921	0.876	0.802	0.725	0.938
$T (^{\circ}\text{C})$	15	$t(\text{ks})$	0.352	1.344	3.116	6.823	15.275	36.769	76.259	156.67					
$\dot{D}(\text{Gy/s})$	0	Lx/Tx	0.911	0.903	0.911	0.917	0.921	0.908	0.917	0.914					
$T (^{\circ}\text{C})$	15	$t(\text{ks})$	0.351	1.311	3.082	6.757	15.328	36.822	76.311	156.72					
$\dot{D}(\text{Gy/s})$	0	Lx/Tx	0.919	0.917	0.911	0.902	0.909	0.908	0.913	0.912					
$T (^{\circ}\text{C})$	15	$t(\text{ks})$	0.352	1.280	3.051	6.693	15.382	36.876	76.365	156.78					
$\dot{D}(\text{Gy/s})$	0	Lx/Tx	0.889	0.896	0.894	0.900	0.907	0.898	0.900	0.893					
$T (^{\circ}\text{C})$	15	$t(\text{ks})$	0.352	1.222	2.961	6.570	15.378	36.872	76.361	156.77					
$\dot{D}(\text{Gy/s})$	0	Lx/Tx	0.912	0.917	0.926	0.919	0.917	0.916	0.912	0.907					

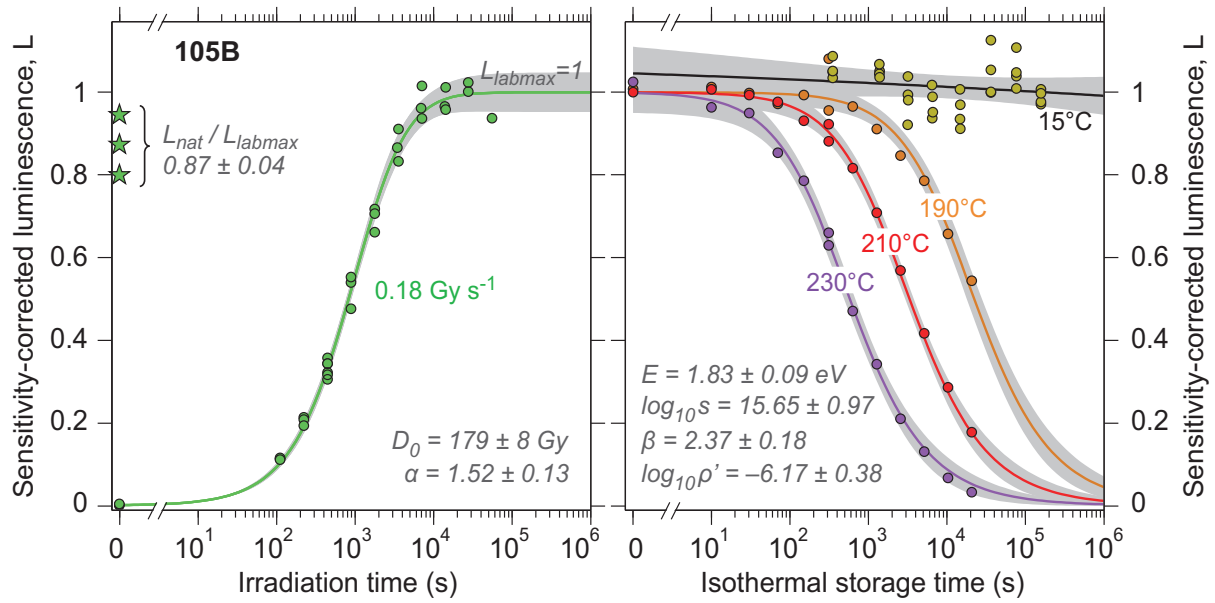


Figure S6-3. Characterisation of electron trapping and detrapping kinetics (105B). Radiation-induced growth (circles, left panel) and isothermal decay (circles, right panel) of sample 105B. Stars in left panel denote natural luminescence levels. Note that the y-axis of the shown data and its simultaneous best-fits are arbitrarily rescaled for convenience of presentation (laboratory saturation at $L=1$ in left panel; initial luminescence of $L=1$ in right panel).

Table S6-3. Characterisation of electron trapping and detrapping kinetics (105B).

105B																
$T (^{\circ}\text{C})$	15	$t (\text{ks})$	Nat	0.111	0.222	0.444	0.889	1.778	3.472	6.944	13.889	27.778	55.556	0.000	0.444	27.778
$\dot{D} (\text{Gy/s})$	0.18	Lx/Tx	4.319	0.516	0.976	1.568	2.464	3.279	3.960	4.394	4.410	4.575	4.283	0.003	1.630	4.678
$T (^{\circ}\text{C})$	15	$t (\text{ks})$	Nat	0.111	0.222	0.444	0.889	1.778	3.556	7.111	14.222	0.000	0.444			
$\dot{D} (\text{Gy/s})$	0.18	Lx/Tx	4.154	0.551	0.987	1.532	2.631	3.360	3.964	4.454	4.813	0.009	1.632			
$T (^{\circ}\text{C})$	15	$t (\text{ks})$	Nat	0.111	0.222	0.444	0.889	1.778	3.556	7.111	14.222	0.000	0.444			
$\dot{D} (\text{Gy/s})$	0.18	Lx/Tx	3.896	0.541	0.943	1.489	2.320	3.223	4.439	4.950	4.668	0.021	1.543			
$T (^{\circ}\text{C})$	230	$t (\text{ks})$	0.000	0.010	0.030	0.070	0.150	0.310	0.630	1.270	2.550	5.110	10.230	20.470	0.310	
$\dot{D} (\text{Gy/s})$	0	Lx/Tx	0.923	0.867	0.855	0.769	0.707	0.567	0.424	0.308	0.189	0.117	0.060	0.029	0.595	
$T (^{\circ}\text{C})$	210	$t (\text{ks})$	0.000	0.010	0.030	0.070	0.150	0.310	0.630	1.270	2.550	5.110	10.230	20.470	0.310	
$\dot{D} (\text{Gy/s})$	0	Lx/Tx	0.930	0.936	0.923	0.908	0.866	0.819	0.759	0.659	0.529	0.388	0.266	0.166	0.858	
$T (^{\circ}\text{C})$	190	$t (\text{ks})$	0.000	0.010	0.030	0.070	0.150	0.310	0.630	1.270	2.550	5.110	10.230	20.470	0.310	
$\dot{D} (\text{Gy/s})$	0	Lx/Tx	0.886	0.889	0.877	0.854	0.872	0.840	0.848	0.800	0.744	0.690	0.577	0.478	0.950	
$T (^{\circ}\text{C})$	15	$t (\text{ks})$	0.350	1.380	3.158	6.435	14.587	36.043	75.494	155.87						
$\dot{D} (\text{Gy/s})$	0	Lx/Tx	1.004	1.006	0.951	0.897	0.895	1.078	0.995	0.929						
$T (^{\circ}\text{C})$	15	$t (\text{ks})$	0.350	1.369	3.137	6.407	14.543	35.983	75.420	155.78						
$\dot{D} (\text{Gy/s})$	0	Lx/Tx	0.929	0.938	0.828	0.914	0.905	0.947	0.941	0.877						
$T (^{\circ}\text{C})$	15	$t (\text{ks})$	0.350	1.379	3.187	6.540	14.692	36.149	75.599	155.98						
$\dot{D} (\text{Gy/s})$	0	Lx/Tx	0.973	0.959	0.908	0.881	0.897	0.925	1.025	0.932						
$T (^{\circ}\text{C})$	15	$t (\text{ks})$	0.349	1.368	3.164	6.507	14.643	36.083	75.520	155.88						
$\dot{D} (\text{Gy/s})$	0	Lx/Tx	1.003	0.984	0.957	0.911	0.840	0.923	0.930	0.919						

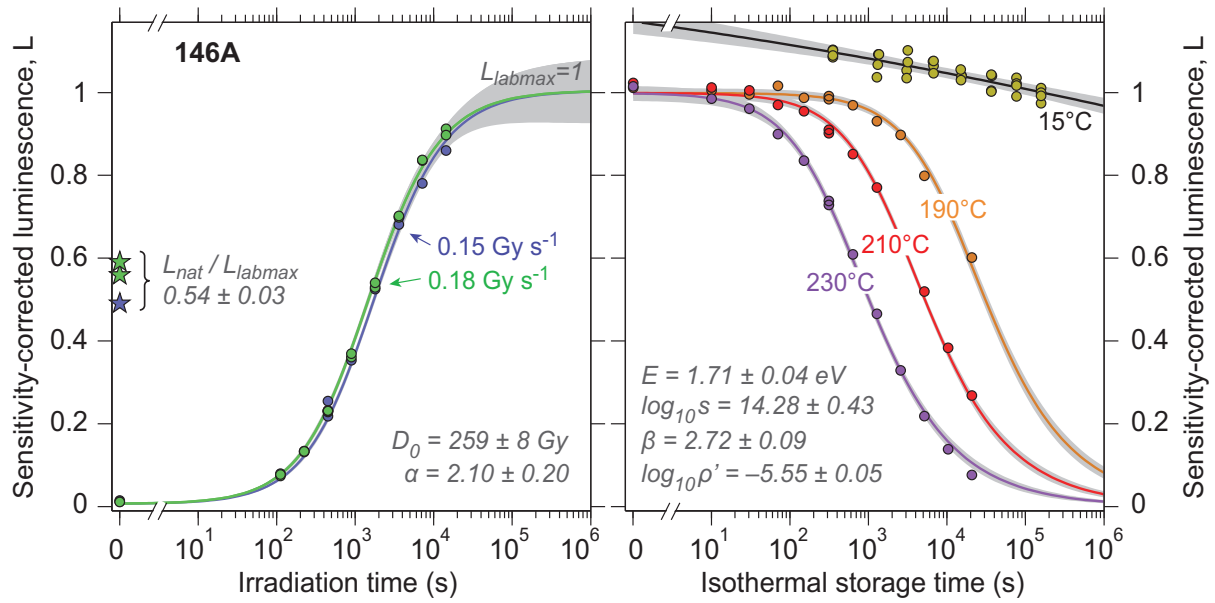


Figure S6-4. Characterisation of electron trapping and detrapping kinetics (146A). Radiation-induced growth (circles, left panel) and isothermal decay (circles, right panel) of sample 146A. Stars in left panel denote natural luminescence levels. Note that the y-axis of the shown data and its simultaneous best-fits are arbitrarily rescaled for convenience of presentation (laboratory saturation at $L=1$ in left panel; initial luminescence of $L=1$ in right panel).

Table S6-4. Characterisation of electron trapping and detrapping kinetics (146A).

146A															
$T (^{\circ}\text{C})$	15	$t (\text{ks})$	Nat	0.111	0.222	0.444	0.889	1.778	3.556	7.111	14.222	0.000	0.444		
$\dot{D} (\text{Gy/s})$	0.18	Lx/Tx	3.940	0.479	0.908	1.581	2.528	3.728	4.937	5.914	6.464	0.039	1.601		
$T (^{\circ}\text{C})$	15	$t (\text{ks})$	Nat	0.111	0.222	0.444	0.889	1.778	3.556	7.111	14.222	0.000	0.444		
$\dot{D} (\text{Gy/s})$	0.18	Lx/Tx	4.121	0.499	0.892	1.581	2.562	3.770	4.904	5.860	6.285	0.032	1.593		
$T (^{\circ}\text{C})$	15	$t (\text{ks})$	Nat	0.111	0.222	0.444	0.889	1.778	3.556	7.111	14.222	0.000	0.444		
$\dot{D} (\text{Gy/s})$	0.153	Lx/Tx	3.603	0.541	0.932	1.847	2.585	3.865	5.030	5.769	6.356	0.058	1.578		
$T (^{\circ}\text{C})$	230	$t (\text{ks})$	0.000	0.010	0.030	0.070	0.150	0.310	0.630	1.270	2.550	5.110	10.230	20.470	0.310
$\dot{D} (\text{Gy/s})$	0	Lx/Tx	0.974	0.946	0.923	0.864	0.802	0.699	0.584	0.447	0.316	0.209	0.132	0.073	0.709
$T (^{\circ}\text{C})$	210	$t (\text{ks})$	0.000	0.010	0.030	0.070	0.150	0.310	0.630	1.270	2.550	5.110	10.230	20.470	0.310
$\dot{D} (\text{Gy/s})$	0	Lx/Tx	1.004	0.993	0.986	0.952	0.937	0.893	0.835	0.756	0.631	0.509	0.376	0.262	0.885
$T (^{\circ}\text{C})$	190	$t (\text{ks})$	0.000	0.010	0.030	0.070	0.150	0.310	0.630	1.270	2.550	5.110	10.230	20.470	0.310
$\dot{D} (\text{Gy/s})$	0	Lx/Tx	0.966	0.961	0.951	0.971	0.943	0.940	0.926	0.889	0.857	0.763	0.684	0.575	0.947
$T (^{\circ}\text{C})$	15	$t (\text{ks})$	0.351	1.267	3.018	6.602	15.201	36.650	76.092	156.46					
$\dot{D} (\text{Gy/s})$	0	Lx/Tx	0.980	0.936	0.951	0.971	0.940	0.940	0.935	0.913					
$T (^{\circ}\text{C})$	15	$t (\text{ks})$	0.351	1.295	3.045	6.659	15.152	36.602	76.043	156.41					
$\dot{D} (\text{Gy/s})$	0	Lx/Tx	0.980	0.948	0.918	0.946	0.923	0.926	0.907	0.887					
$T (^{\circ}\text{C})$	15	$t (\text{ks})$	0.351	1.320	3.119	6.722	14.909	36.385	75.815	156.17					
$\dot{D} (\text{Gy/s})$	0	Lx/Tx	0.974	0.965	0.949	0.951	0.911	0.888	0.899	0.861					
$T (^{\circ}\text{C})$	15	$t (\text{ks})$	0.350	1.341	3.136	6.681	14.817	36.257	75.693	156.05					
$\dot{D} (\text{Gy/s})$	0	Lx/Tx	0.984	0.985	0.994	0.944	0.953	0.904	0.894	0.895					

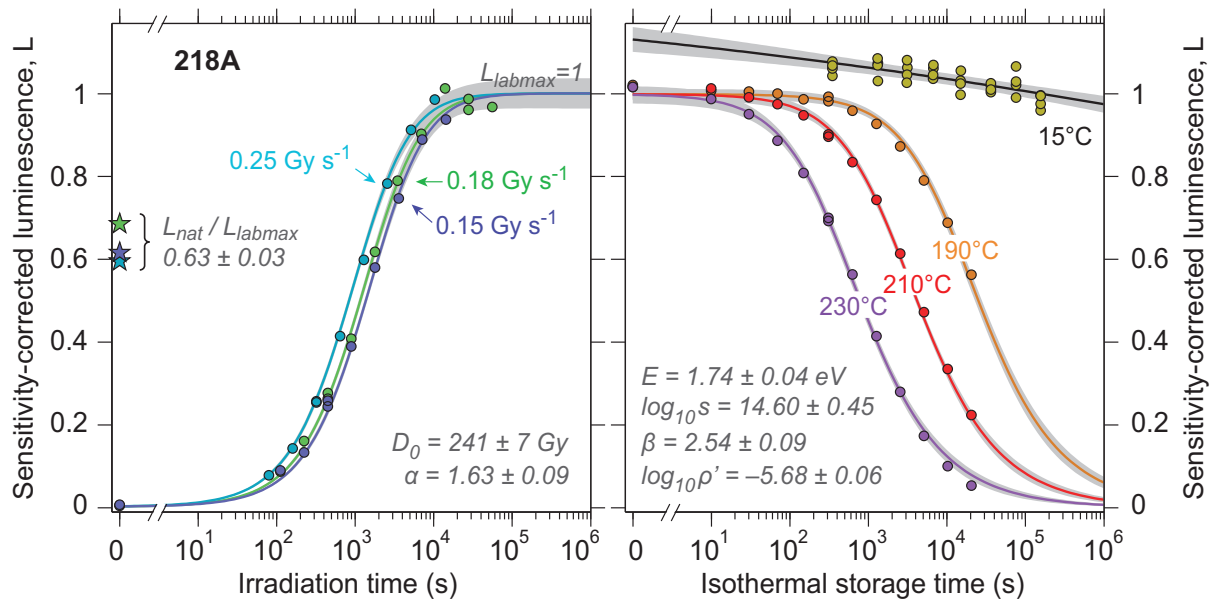


Figure S6-5. Characterisation of electron trapping and detrapping kinetics (218A). Radiation-induced growth (circles, left panel) and isothermal decay (circles, right panel) of sample 218A. Stars in left panel denote natural luminescence levels. Note that the y-axis of the shown data and its simultaneous best-fits are arbitrarily rescaled for convenience of presentation (laboratory saturation at $L=1$ in left panel; initial luminescence of $L=1$ in right panel).

Table S6-5. Characterisation of electron trapping and detrapping kinetics (218A).

218A																
$T(^{\circ}\text{C})$	15	$t(\text{ks})$	Nat	0.080	0.160	0.320	0.640	1.280	2.560	5.120	10.240	0.000	0.320			
$\dot{D}(\text{Gy/s})$	0.25	Lx/Tx	3.714	0.475	0.881	1.575	2.581	3.736	4.894	5.705	6.168	0.015	1.596			
$T(^{\circ}\text{C})$	15	$t(\text{ks})$	Nat	0.111	0.222	0.444	0.889	1.778	3.472	6.944	13.889	27.778	55.556	0.000	0.444	27.778
$\dot{D}(\text{Gy/s})$	0.18	Lx/Tx	3.926	0.489	0.910	1.500	2.333	3.540	4.532	5.181	5.811	5.512	5.554	0.018	1.578	5.664
$T(^{\circ}\text{C})$	15	$t(\text{ks})$	Nat	0.111	0.222	0.444	0.889	1.778	3.556	7.111	14.222	0.000	0.444			
$\dot{D}(\text{Gy/s})$	0.153	Lx/Tx	4.006	0.568	0.858	1.670	2.528	3.770	4.861	5.789	6.107	0.032	1.582			
$T(^{\circ}\text{C})$	230	$t(\text{ks})$	0.000	0.010	0.030	0.070	0.150	0.310	0.630	1.270	2.550	5.110	10.230	20.470	0.310	
$\dot{D}(\text{Gy/s})$	0	Lx/Tx	0.970	0.942	0.907	0.846	0.772	0.661	0.537	0.395	0.267	0.165	0.095	0.050	0.668	
$T(^{\circ}\text{C})$	210	$t(\text{ks})$	0.000	0.010	0.030	0.070	0.150	0.310	0.630	1.270	2.550	5.110	10.230	20.470	0.310	
$\dot{D}(\text{Gy/s})$	0	Lx/Tx	0.990	0.987	0.966	0.950	0.923	0.878	0.813	0.724	0.598	0.460	0.326	0.218	0.873	
$T(^{\circ}\text{C})$	190	$t(\text{ks})$	0.000	0.010	0.030	0.070	0.150	0.310	0.630	1.270	2.550	5.110	10.230	20.470	0.310	
$\dot{D}(\text{Gy/s})$	0	Lx/Tx	0.988	0.975	0.973	0.969	0.955	0.951	0.928	0.897	0.845	0.765	0.666	0.545	0.962	
$T(^{\circ}\text{C})$	15	$t(\text{ks})$	0.351	1.323	3.130	6.745	14.952	36.409	75.859	156.23						
$\dot{D}(\text{Gy/s})$	0	Lx/Tx	0.962	0.991	0.981	0.979	0.921	0.940	0.983	0.886						
$T(^{\circ}\text{C})$	15	$t(\text{ks})$	0.350	1.314	3.109	6.701	14.890	36.329	75.765	156.12						
$\dot{D}(\text{Gy/s})$	0	Lx/Tx	1.142	1.150	1.126	1.115	1.110	1.103	1.099	1.072						
$T(^{\circ}\text{C})$	15	$t(\text{ks})$	0.350	1.322	3.102	6.745	15.028	36.484	75.935	156.31						
$\dot{D}(\text{Gy/s})$	0	Lx/Tx	0.998	0.955	1.001	0.990	0.978	0.930	0.918	0.903						
$T(^{\circ}\text{C})$	15	$t(\text{ks})$	0.349	1.313	3.082	6.701	14.963	36.402	75.838	156.20						
$\dot{D}(\text{Gy/s})$	0	Lx/Tx	1.171	1.189	1.125	1.145	1.123	1.106	1.129	1.091						

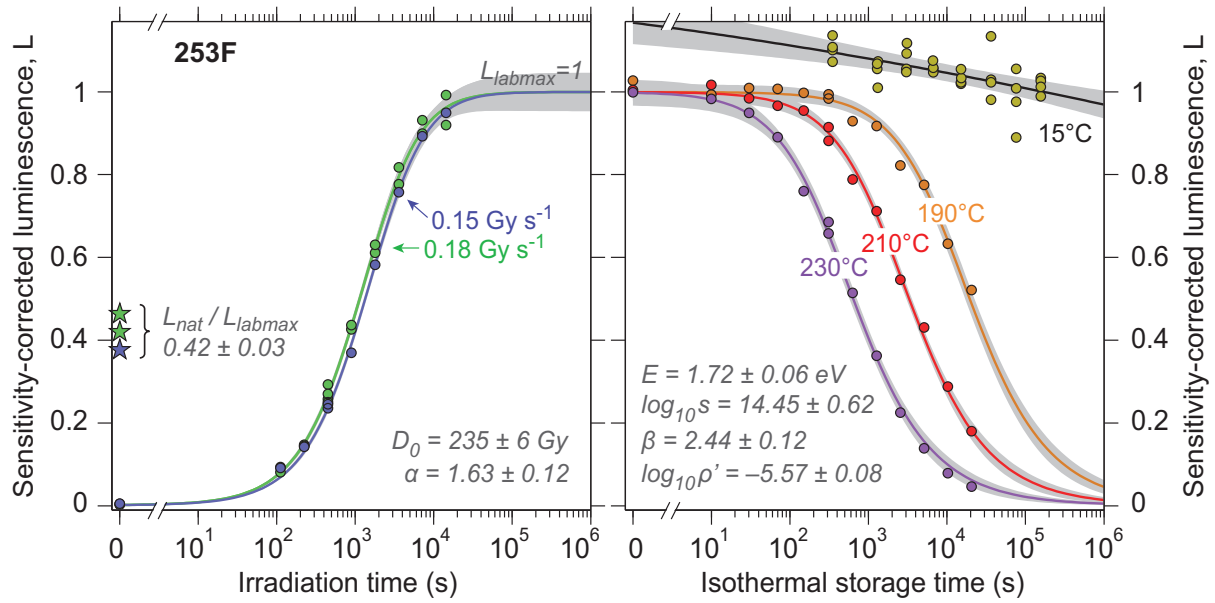


Figure S6-6. Characterisation of electron trapping and detrapping kinetics (253F). Radiation-induced growth (circles, left panel) and isothermal decay (circles, right panel) of sample 253F. Stars in left panel denote natural luminescence levels. Note that the y-axis of the shown data and its simultaneous best-fits are arbitrarily rescaled for convenience of presentation (laboratory saturation at $L=1$ in left panel; initial luminescence of $L=1$ in right panel).

Table S6-6. Characterisation of electron trapping and detrapping kinetics (253F).

253F															
$T (^{\circ}\text{C})$	15	$t (\text{ks})$	Nat	0.111	0.222	0.444	0.889	1.778	3.556	7.111	14.222	0.000	0.444		
$\dot{D} (\text{Gy/s})$	0.18	Lx/Tx	2.842	0.489	0.898	1.579	2.608	3.749	4.767	5.516	6.091	0.020	1.794		
$T (^{\circ}\text{C})$	15	$t (\text{ks})$	Nat	0.111	0.222	0.444	0.889	1.778	3.556	7.111	14.222	0.000	0.444		
$\dot{D} (\text{Gy/s})$	0.18	Lx/Tx	2.573	0.563	0.882	1.649	2.672	3.863	5.010	5.710	5.637	0.007	1.529		
$T (^{\circ}\text{C})$	15	$t (\text{ks})$	Nat	0.111	0.222	0.444	0.889	1.778	3.556	7.111	14.222	0.000	0.444		
$\dot{D} (\text{Gy/s})$	0.153	Lx/Tx	2.601	0.624	0.979	1.626	2.554	4.030	5.243	6.185	6.573	0.024	1.691		
$T (^{\circ}\text{C})$	230	$t (\text{ks})$	0.000	0.010	0.030	0.070	0.150	0.310	0.630	1.270	2.550	5.110	10.230	20.470	0.310
$\dot{D} (\text{Gy/s})$	0	Lx/Tx	0.928	0.913	0.882	0.827	0.706	0.611	0.478	0.336	0.208	0.128	0.073	0.042	0.636
$T (^{\circ}\text{C})$	210	$t (\text{ks})$	0.000	0.010	0.030	0.070	0.150	0.310	0.630	1.270	2.550	5.110	10.230	20.470	0.310
$\dot{D} (\text{Gy/s})$	0	Lx/Tx	0.958	0.970	0.939	0.922	0.911	0.841	0.752	0.679	0.520	0.411	0.274	0.171	0.873
$T (^{\circ}\text{C})$	190	$t (\text{ks})$	0.000	0.010	0.030	0.070	0.150	0.310	0.630	1.270	2.550	5.110	10.230	20.470	0.310
$\dot{D} (\text{Gy/s})$	0	Lx/Tx	0.992	0.960	0.975	0.973	0.964	0.960	0.897	0.887	0.794	0.748	0.611	0.503	0.950
$T (^{\circ}\text{C})$	15	$t (\text{ks})$	0.350	1.323	3.073	6.717	15.106	36.561	76.012	156.39					
$\dot{D} (\text{Gy/s})$	0	Lx/Tx	0.937	0.937	0.976	0.922	0.891	0.857	0.922	0.864					
$T (^{\circ}\text{C})$	15	$t (\text{ks})$	0.349	1.313	3.054	6.673	15.036	36.475	75.911	156.27					
$\dot{D} (\text{Gy/s})$	0	Lx/Tx	0.846	0.752	0.813	0.779	0.761	0.845	0.662	0.769					
$T (^{\circ}\text{C})$	15	$t (\text{ks})$	0.350	1.294	3.045	6.660	15.154	36.610	76.060	156.44					
$\dot{D} (\text{Gy/s})$	0	Lx/Tx	0.938	0.899	0.899	0.901	0.880	0.877	0.859	0.874					
$T (^{\circ}\text{C})$	15	$t (\text{ks})$	0.350	1.286	3.027	6.618	15.081	36.520	75.956	156.32					
$\dot{D} (\text{Gy/s})$	0	Lx/Tx	0.868	0.837	0.821	0.843	0.826	0.801	0.765	0.793					

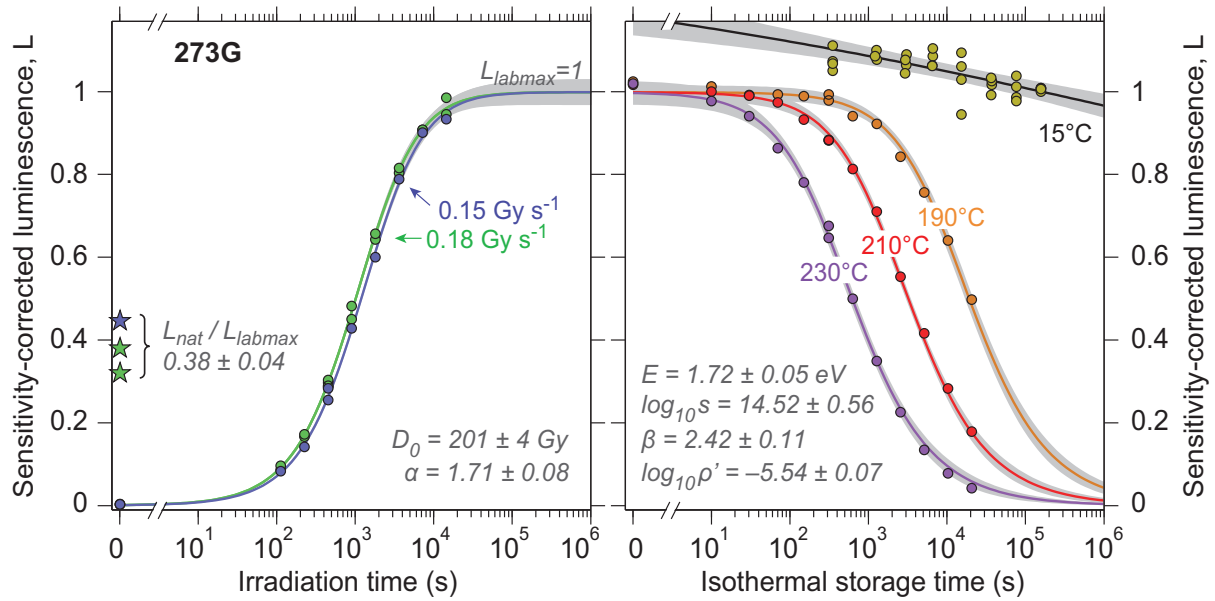


Figure S6-7. Characterisation of electron trapping and detrapping kinetics (273G). Radiation-induced growth (circles, left panel) and isothermal decay (circles, right panel) of sample 273G. Stars in left panel denote natural luminescence levels. Note that the y-axis of the shown data and its simultaneous best-fits are arbitrarily rescaled for convenience of presentation (laboratory saturation at $L=1$ in left panel; initial luminescence of $L=1$ in right panel).

Table S6-7. Characterisation of electron trapping and detrapping kinetics (273G).

273G															
$T (^{\circ}\text{C})$	15	$t (\text{ks})$	Nat	0.111	0.222	0.444	0.889	1.778	3.556	7.111	14.222	0.000	0.444		
$\dot{D} (\text{Gy/s})$	0.18	Lx/Tx	1.791	0.485	0.935	1.602	2.521	3.601	4.501	5.081	5.520	0.018	1.661		
$T (^{\circ}\text{C})$	15	$t (\text{ks})$	Nat	0.111	0.222	0.444	0.889	1.778	3.556	7.111	14.222	0.000	0.444		
$\dot{D} (\text{Gy/s})$	0.18	Lx/Tx	2.055	0.522	0.931	1.564	2.606	3.552	4.411	4.911	5.116	0.011	1.639		
$T (^{\circ}\text{C})$	15	$t (\text{ks})$	Nat	0.111	0.222	0.444	0.889	1.778	3.556	7.111	14.222	0.000	0.444		
$\dot{D} (\text{Gy/s})$	0.153	Lx/Tx	2.795	0.520	0.888	1.599	2.684	3.762	4.943	5.651	5.852	0.017	1.772		
$T (^{\circ}\text{C})$	230	$t (\text{ks})$	0.000	0.010	0.030	0.070	0.150	0.310	0.630	1.270	2.550	5.110	10.230	20.470	0.310
$\dot{D} (\text{Gy/s})$	0	Lx/Tx	0.927	0.889	0.855	0.785	0.710	0.589	0.455	0.317	0.205	0.122	0.070	0.038	0.614
$T (^{\circ}\text{C})$	210	$t (\text{ks})$	0.000	0.010	0.030	0.070	0.150	0.310	0.630	1.270	2.550	5.110	10.230	20.470	0.310
$\dot{D} (\text{Gy/s})$	0	Lx/Tx	0.986	0.970	0.960	0.944	0.904	0.856	0.788	0.688	0.536	0.403	0.274	0.173	0.855
$T (^{\circ}\text{C})$	190	$t (\text{ks})$	0.000	0.010	0.030	0.070	0.150	0.310	0.630	1.270	2.550	5.110	10.230	20.470	0.310
$\dot{D} (\text{Gy/s})$	0	Lx/Tx	0.962	0.950	0.932	0.933	0.929	0.919	0.883	0.866	0.791	0.710	0.601	0.467	0.933
$T (^{\circ}\text{C})$	15	$t (\text{ks})$	0.350	1.265	3.015	6.601	15.201	36.657	76.108	156.48					
$\dot{D} (\text{Gy/s})$	0	Lx/Tx	0.919	0.922	0.933	0.929	0.908	0.870	0.844	0.856					
$T (^{\circ}\text{C})$	15	$t (\text{ks})$	0.350	1.260	3.001	6.565	15.128	36.567	76.003	156.36					
$\dot{D} (\text{Gy/s})$	0	Lx/Tx	0.886	0.928	0.898	0.932	0.923	0.837	0.824	0.851					
$T (^{\circ}\text{C})$	15	$t (\text{ks})$	0.350	1.211	2.932	6.491	15.196	36.651	76.102	156.48					
$\dot{D} (\text{Gy/s})$	0	Lx/Tx	0.915	0.931	0.923	0.912	0.883	0.880	0.890	0.864					
$T (^{\circ}\text{C})$	15	$t (\text{ks})$	0.350	1.207	2.921	6.457	15.121	36.560	75.995	156.36					
$\dot{D} (\text{Gy/s})$	0	Lx/Tx	0.948	1.002	0.891	0.907	0.806	0.882	0.864	0.859					

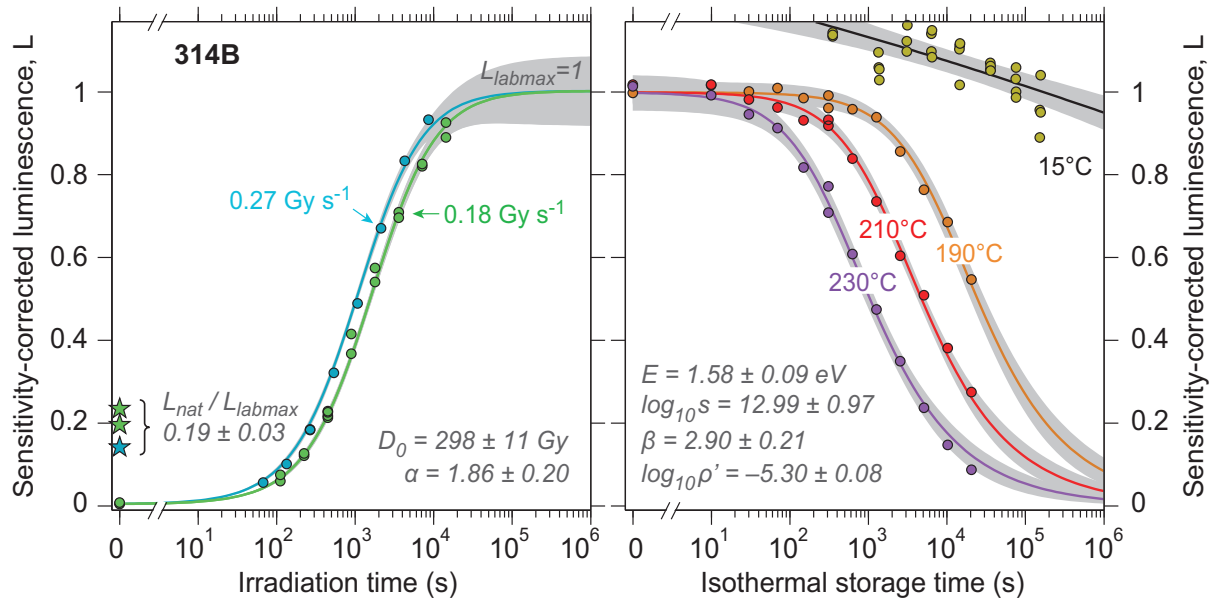


Figure S6-8. Characterisation of electron trapping and detrapping kinetics (314B). Radiation-induced growth (circles, left panel) and isothermal decay (circles, right panel) of sample 314B. Stars in left panel denote natural luminescence levels. Note that the y-axis of the shown data and its simultaneous best-fits are arbitrarily rescaled for convenience of presentation (laboratory saturation at $L=1$ in left panel; initial luminescence of $L=1$ in right panel).

Table S6-8. Characterisation of electron trapping and detrapping kinetics (314B).

314B															
$T (^{\circ}\text{C})$	15	$t (\text{ks})$	Nat	0.067	0.133	0.267	0.533	1.067	2.133	4.267	8.533	0.000	0.267		
$\dot{D} (\text{Gy/s})$	0.27	Lx/Tx	1.299	0.498	0.915	1.706	3.000	4.577	6.288	7.832	8.768	0.018	1.689		
$T (^{\circ}\text{C})$	15	$t (\text{ks})$	Nat	0.111	0.222	0.444	0.889	1.778	3.556	7.111	14.222	0.000	0.444		
$\dot{D} (\text{Gy/s})$	0.18	Lx/Tx	1.800	0.434	0.916	1.628	3.214	4.455	5.507	6.371	6.914	0.004	1.670		
$T (^{\circ}\text{C})$	15	$t (\text{ks})$	Nat	0.111	0.222	0.444	0.889	1.778	3.556	7.111	14.222	0.000	0.444		
$\dot{D} (\text{Gy/s})$	0.18	Lx/Tx	1.428	0.528	0.914	1.659	2.712	4.007	5.162	6.131	6.872	0.029	1.679		
$T (^{\circ}\text{C})$	230	$t (\text{ks})$	0.000	0.010	0.030	0.070	0.150	0.310	0.630	1.270	2.550	5.110	10.230	20.470	0.310
$\dot{D} (\text{Gy/s})$	0	Lx/Tx	0.927	0.908	0.866	0.835	0.748	0.648	0.556	0.434	0.320	0.217	0.134	0.079	0.706
$T (^{\circ}\text{C})$	210	$t (\text{ks})$	0.000	0.010	0.030	0.070	0.150	0.310	0.630	1.270	2.550	5.110	10.230	20.470	0.310
$\dot{D} (\text{Gy/s})$	0	Lx/Tx	0.972	0.972	0.938	0.918	0.889	0.876	0.801	0.701	0.576	0.485	0.364	0.262	0.890
$T (^{\circ}\text{C})$	190	$t (\text{ks})$	0.000	0.010	0.030	0.070	0.150	0.310	0.630	1.270	2.550	5.110	10.230	20.470	0.310
$\dot{D} (\text{Gy/s})$	0	Lx/Tx	0.994	1.012	0.997	1.005	0.982	0.988	0.955	0.935	0.853	0.761	0.683	0.544	0.957
$T (^{\circ}\text{C})$	15	$t (\text{ks})$	0.352	1.359	3.092	6.368	14.521	35.978	75.429	152.20					
$\dot{D} (\text{Gy/s})$	0	Lx/Tx	1.034	0.958	1.015	1.031	1.006	0.967	0.904	0.864					
$T (^{\circ}\text{C})$	15	$t (\text{ks})$	0.352	1.348	3.071	6.341	14.479	35.920	75.355	155.72					
$\dot{D} (\text{Gy/s})$	0	Lx/Tx	1.133	1.059	1.062	1.062	1.066	1.018	0.997	0.919					
$T (^{\circ}\text{C})$	15	$t (\text{ks})$	0.352	1.384	3.146	6.476	14.629	36.086	75.537	152.31					
$\dot{D} (\text{Gy/s})$	0	Lx/Tx	1.021	0.926	1.045	1.034	1.005	0.956	0.953	0.801					
$T (^{\circ}\text{C})$	15	$t (\text{ks})$	0.352	1.373	3.123	6.444	14.582	36.022	75.458	155.82					
$\dot{D} (\text{Gy/s})$	0	Lx/Tx	1.039	0.964	1.125	0.990	0.929	0.960	0.901	0.950					

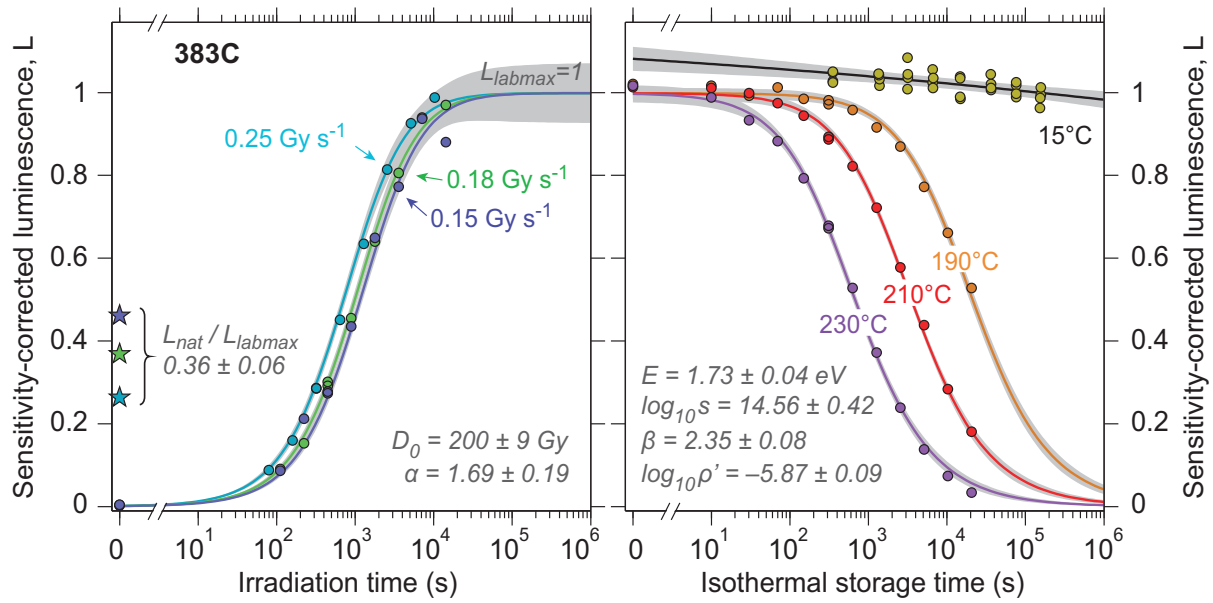


Figure S6-9. Characterisation of electron trapping and detrapping kinetics (383C). Radiation-induced growth (circles, left panel) and isothermal decay (circles, right panel) of sample 383C. Stars in left panel denote natural luminescence levels. Note that the y-axis of the shown data and its simultaneous best-fits are arbitrarily rescaled for convenience of presentation (laboratory saturation at $L=1$ in left panel; initial luminescence of $L=1$ in right panel).

Table S6-9. Characterisation of electron trapping and detrapping kinetics (383C).

383C															
T (°C)	15	t (ks)	Nat	0.080	0.160	0.320	0.640	1.280	2.560	5.120	10.240	0.000	0.320		
\dot{D} (Gy/s)	0.25	Lx/Tx	1.426	0.473	0.866	1.548	2.445	3.439	4.413	5.021	5.357	0.012	1.548		
T (°C)	15	t (ks)	Nat	0.111	0.222	0.444	0.889	1.778	3.556	7.111	14.222	0.000	0.444		
\dot{D} (Gy/s)	0.18	Lx/Tx	1.926	0.472	0.801	1.526	2.381	3.350	4.216	4.917	5.078	0.017	1.575		
T (°C)	15	t (ks)	Nat	0.111	0.222	0.444	0.889	1.778	3.556	7.111	14.222	0.000	0.444		
\dot{D} (Gy/s)	0.153	Lx/Tx	2.653	0.500	1.219	1.596	2.503	3.734	4.448	5.392	5.068	0.023	1.573		
T (°C)	230	t (ks)	0.000	0.010	0.030	0.070	0.150	0.310	0.630	1.270	2.550	5.110	10.230	20.470	0.310
\dot{D} (Gy/s)	0	Lx/Tx	0.958	0.930	0.879	0.831	0.746	0.633	0.497	0.351	0.225	0.130	0.070	0.032	0.638
T (°C)	210	t (ks)	0.000	0.010	0.030	0.070	0.150	0.310	0.630	1.270	2.550	5.110	10.230	20.470	0.310
\dot{D} (Gy/s)	0	Lx/Tx	0.976	0.974	0.961	0.939	0.909	0.854	0.792	0.695	0.556	0.422	0.273	0.174	0.860
T (°C)	190	t (ks)	0.000	0.010	0.030	0.070	0.150	0.310	0.630	1.270	2.550	5.110	10.230	20.470	0.310
\dot{D} (Gy/s)	0	Lx/Tx	0.975	0.971	0.948	0.967	0.941	0.938	0.915	0.874	0.830	0.738	0.632	0.504	0.928
T (°C)	15	t (ks)	0.353	1.384	3.171	6.584	14.737	36.193	75.644	152.42					
\dot{D} (Gy/s)	0	Lx/Tx	1.002	0.991	1.010	1.029	1.013	0.995	0.993	0.939					
T (°C)	15	t (ks)	0.352	1.373	3.148	6.547	14.684	36.125	75.560	155.92					
\dot{D} (Gy/s)	0	Lx/Tx	1.005	0.990	0.967	0.982	0.992	1.002	0.948	0.954					
T (°C)	15	t (ks)	0.353	1.356	3.167	6.663	14.816	36.273	75.723	152.50					
\dot{D} (Gy/s)	0	Lx/Tx	1.019	1.010	1.012	1.004	0.955	0.976	0.994	0.956					
T (°C)	15	t (ks)	0.352	1.345	3.146	6.621	14.759	36.200	75.635	156.00					
\dot{D} (Gy/s)	0	Lx/Tx	1.002	1.023	1.061	0.988	0.968	0.988	0.975	0.990					

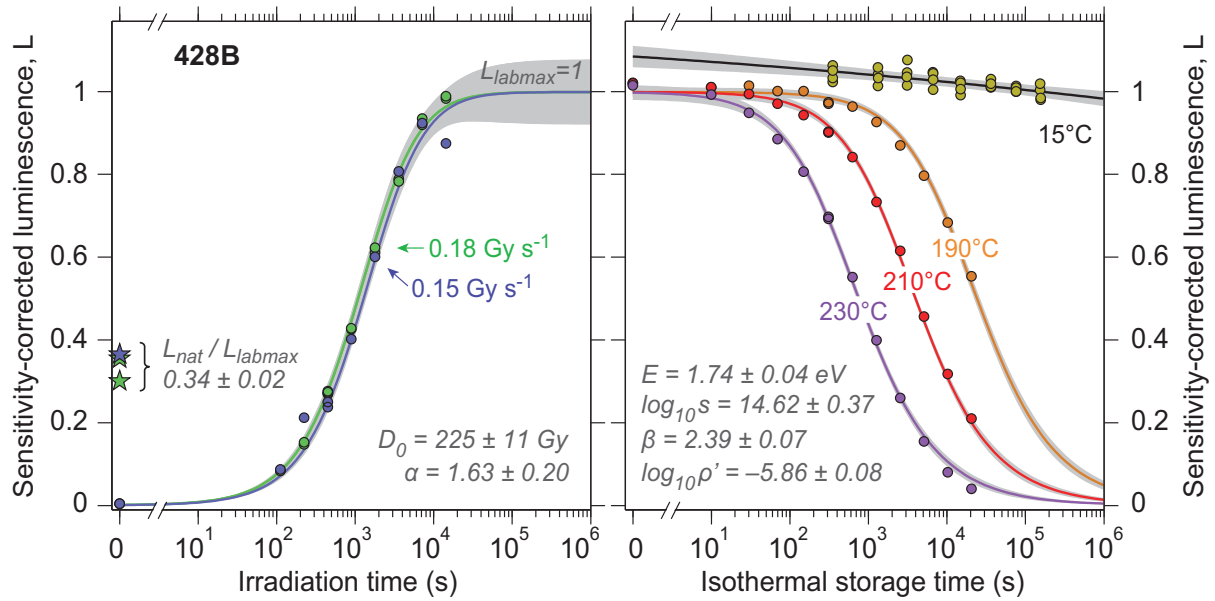


Figure S6-10. Characterisation of electron trapping and detrapping kinetics (428B). Radiation-induced growth (circles, left panel) and isothermal decay (circles, right panel) of sample 428B. Stars in left panel denote natural luminescence levels. Note that the y-axis of the shown data and its simultaneous best-fits are arbitrarily rescaled for convenience of presentation (laboratory saturation at $L=1$ in left panel; initial luminescence of $L=1$ in right panel).

Table S6-10. Characterisation of electron trapping and detrapping kinetics (428B).

428B															
$T (^{\circ}\text{C})$	15	$t (\text{ks})$	Nat	0.111	0.222	0.444	0.889	1.778	3.556	7.111	14.222	0.000	0.444		
$\dot{D} (\text{Gy/s})$	0.18	Lx/Tx	1.758	0.493	0.864	1.581	2.495	3.578	4.622	5.477	5.761	0.024	1.581		
$T (^{\circ}\text{C})$	15	$t (\text{ks})$	Nat	0.111	0.222	0.444	0.889	1.778	3.556	7.111	14.222	0.000	0.444		
$\dot{D} (\text{Gy/s})$	0.18	Lx/Tx	2.055	0.482	0.883	1.597	2.478	3.609	4.533	5.328	5.727	0.023	1.582		
$T (^{\circ}\text{C})$	15	$t (\text{ks})$	Nat	0.111	0.222	0.444	0.889	1.778	3.556	7.111	14.222	0.000	0.444		
$\dot{D} (\text{Gy/s})$	0.153	Lx/Tx	2.302	0.548	1.336	1.500	2.535	3.786	5.090	5.830	5.517	0.027	1.577		
$T (^{\circ}\text{C})$	230	$t (\text{ks})$	0.000	0.010	0.030	0.070	0.150	0.310	0.630	1.270	2.550	5.110	10.230	20.470	0.310
$\dot{D} (\text{Gy/s})$	0	Lx/Tx	0.982	0.961	0.919	0.857	0.781	0.670	0.534	0.386	0.251	0.150	0.077	0.039	0.676
$T (^{\circ}\text{C})$	210	$t (\text{ks})$	0.000	0.010	0.030	0.070	0.150	0.310	0.630	1.270	2.550	5.110	10.230	20.470	0.310
$\dot{D} (\text{Gy/s})$	0	Lx/Tx	0.982	0.974	0.958	0.935	0.908	0.867	0.810	0.706	0.593	0.439	0.305	0.202	0.870
$T (^{\circ}\text{C})$	190	$t (\text{ks})$	0.000	0.010	0.030	0.070	0.150	0.310	0.630	1.270	2.550	5.110	10.230	20.470	0.310
$\dot{D} (\text{Gy/s})$	0	Lx/Tx	0.993	0.982	0.986	0.973	0.973	0.947	0.937	0.900	0.846	0.774	0.665	0.538	0.944
$T (^{\circ}\text{C})$	15	$t (\text{ks})$	0.352	1.327	3.138	6.687	14.894	36.351	75.801	152.58					
$\dot{D} (\text{Gy/s})$	0	Lx/Tx	0.959	0.976	1.008	0.941	0.929	0.965	0.950	0.940					
$T (^{\circ}\text{C})$	15	$t (\text{ks})$	0.352	1.318	3.118	6.643	14.833	36.275	75.710	156.07					
$\dot{D} (\text{Gy/s})$	0	Lx/Tx	1.040	0.991	1.022	1.023	1.004	0.988	0.977	0.958					
$T (^{\circ}\text{C})$	15	$t (\text{ks})$	0.352	1.327	3.110	6.712	14.973	36.430	75.881	152.66					
$\dot{D} (\text{Gy/s})$	0	Lx/Tx	1.002	1.003	0.985	1.014	0.991	0.981	0.980	0.990					
$T (^{\circ}\text{C})$	15	$t (\text{ks})$	0.352	1.318	3.091	6.668	14.909	36.351	75.786	156.15					
$\dot{D} (\text{Gy/s})$	0	Lx/Tx	1.050	1.057	1.035	1.028	1.005	1.018	0.999	0.984					

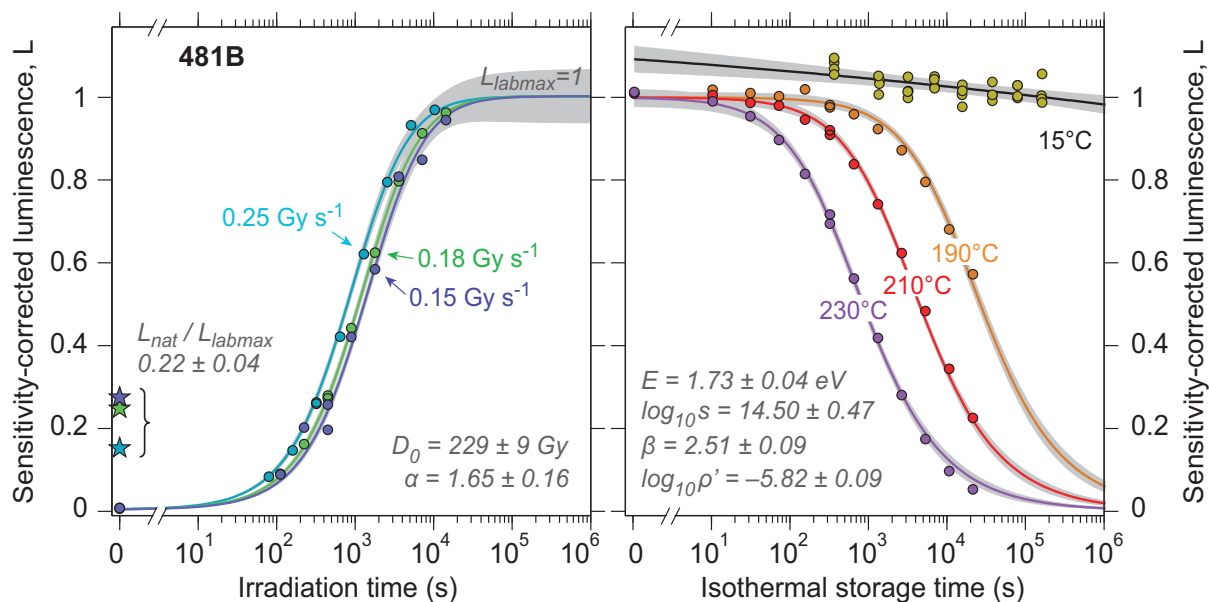


Figure S6-11. Characterisation of electron trapping and detrapping kinetics (481B). Radiation-induced growth (circles, left panel) and isothermal decay (circles, right panel) of sample 481B. Stars in left panel denote natural luminescence levels. Note that the y-axis of the shown data and its simultaneous best-fits are arbitrarily rescaled for convenience of presentation (laboratory saturation at $L=1$ in left panel; initial luminescence of $L=1$ in right panel).

Table S6-11. Characterisation of electron trapping and detrapping kinetics (481B).

481B															
T (°C)	15	t (ks)	Nat	0.080	0.160	0.320	0.640	1.280	2.560	5.120	10.240	0.000	0.320		
\dot{D} (Gy/s)	0.25	L_x/T_x	0.897	0.483	0.867	1.549	2.537	3.745	4.799	5.632	5.862	0.014	1.570		
T (°C)	15	t (ks)	Nat	0.111	0.222	0.444	0.889	1.778	3.556	7.111	14.222	0.000	0.444		
\dot{D} (Gy/s)	0.18	L_x/T_x	1.386	0.490	0.898	1.526	2.490	3.524	4.504	5.163	5.447	0.023	1.564		
T (°C)	15	t (ks)	Nat	0.111	0.222	0.444	0.889	1.778	3.556	7.111	14.222	0.000	0.444		
\dot{D} (Gy/s)	0.153	L_x/T_x	1.645	0.514	1.202	1.171	2.532	3.529	4.885	5.134	5.717	0.021	1.539		
T (°C)	230	t (ks)	0.000	0.010	0.030	0.070	0.150	0.310	0.630	1.270	2.550	5.110	10.230	20.470	0.310
\dot{D} (Gy/s)	0	L_x/T_x	0.975	0.953	0.919	0.863	0.784	0.668	0.540	0.402	0.270	0.167	0.092	0.050	0.690
T (°C)	210	t (ks)	0.000	0.010	0.030	0.070	0.150	0.310	0.630	1.270	2.550	5.110	10.230	20.470	0.310
\dot{D} (Gy/s)	0	L_x/T_x	0.981	0.978	0.959	0.953	0.920	0.884	0.815	0.721	0.606	0.469	0.334	0.218	0.895
T (°C)	190	t (ks)	0.000	0.010	0.030	0.070	0.150	0.310	0.630	1.270	2.550	5.110	10.230	20.470	0.310
\dot{D} (Gy/s)	0	L_x/T_x	0.983	0.992	0.983	0.976	0.993	0.950	0.934	0.899	0.849	0.775	0.663	0.557	0.955
T (°C)	15	t (ks)	0.353	1.327	3.082	6.709	15.053	36.510	75.960	152.73					
\dot{D} (Gy/s)	0	L_x/T_x	1.010	0.970	0.946	0.979	0.911	0.937	0.959	0.936					
T (°C)	15	t (ks)	0.352	1.319	3.064	6.667	14.985	36.426	75.861	156.22					
\dot{D} (Gy/s)	0	L_x/T_x	1.040	1.005	0.971	0.998	0.979	0.965	1.001	1.028					
T (°C)	15	t (ks)	0.353	1.299	3.053	6.676	15.102	36.559	76.010	152.78					
\dot{D} (Gy/s)	0	L_x/T_x	1.032	0.948	0.989	0.962	0.970	0.948	0.940	0.939					
T (°C)	15	t (ks)	0.352	1.291	3.037	6.637	15.033	36.474	75.910	156.27					
\dot{D} (Gy/s)	0	L_x/T_x	1.034	1.031	0.993	1.022	0.996	1.016	0.983	0.968					

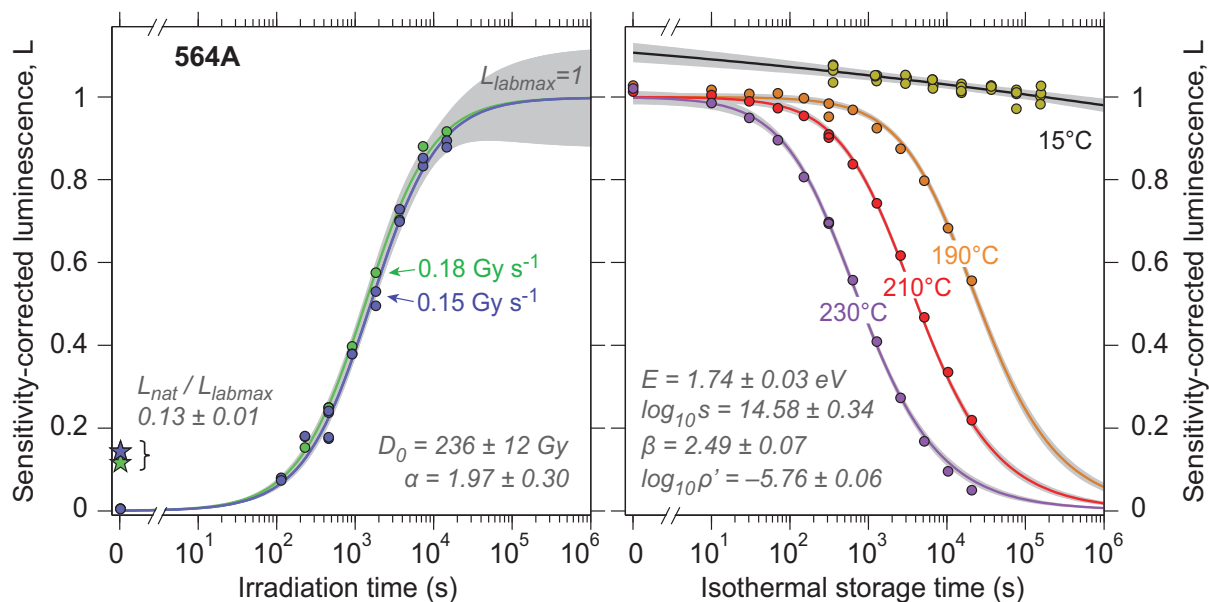


Figure S6-12. Characterisation of electron trapping and detrapping kinetics (564A). Radiation-induced growth (circles, left panel) and isothermal decay (circles, right panel) of sample 564A. Stars in left panel denote natural luminescence levels. Note that the y-axis of the shown data and its simultaneous best-fits are arbitrarily rescaled for convenience of presentation (laboratory saturation at $L=1$ in left panel; initial luminescence of $L=1$ in right panel).

Table S6-12. Characterisation of electron trapping and detrapping kinetics (564A).

564A															
T (°C)	15	t (ks)	Nat	0.111	0.222	0.444	0.889	1.778	3.556	7.111	14.222	0.000	0.444		
\dot{D} (Gy/s)	0.18	Lx/Tx	0.728	0.493	0.963	1.569	2.496	3.612	4.411	5.529	5.756	0.032	1.566		
T (°C)	15	t (ks)	Nat	0.111	0.222	0.444	0.889	1.778	3.556	7.111	14.222	0.000	0.444		
\dot{D} (Gy/s)	0.153	Lx/Tx	0.950	0.528	1.186	1.152	2.505	3.274	4.819	5.504	5.914	0.035	1.568		
T (°C)	15	t (ks)	Nat	0.111	0.222	0.444	0.889	1.778	3.556	7.111	14.222	0.000	0.444		
\dot{D} (Gy/s)	0.153	Lx/Tx	0.963	0.494	1.214	1.198	2.546	3.562	4.703	5.731	5.906	0.031	1.621		
T (°C)	230	t (ks)	0.000	0.010	0.030	0.070	0.150	0.310	0.630	1.270	2.550	5.110	10.230	20.470	0.310
\dot{D} (Gy/s)	0	Lx/Tx	0.973	0.940	0.905	0.854	0.769	0.662	0.531	0.389	0.260	0.159	0.090	0.047	0.665
T (°C)	210	t (ks)	0.000	0.010	0.030	0.070	0.150	0.310	0.630	1.270	2.550	5.110	10.230	20.470	0.310
\dot{D} (Gy/s)	0	Lx/Tx	0.982	0.974	0.959	0.943	0.925	0.874	0.812	0.720	0.597	0.453	0.324	0.211	0.881
T (°C)	190	t (ks)	0.000	0.010	0.030	0.070	0.150	0.310	0.630	1.270	2.550	5.110	10.230	20.470	0.310
\dot{D} (Gy/s)	0	Lx/Tx	1.022	1.011	1.003	1.004	0.992	0.979	0.963	0.919	0.870	0.793	0.679	0.553	0.947
T (°C)	15	t (ks)	0.352	1.270	3.025	6.619	15.153	36.610	76.060	152.83					
\dot{D} (Gy/s)	0	Lx/Tx	0.979	0.995	0.990	0.972	0.975	0.970	0.962	0.947					
T (°C)	15	t (ks)	0.352	1.264	3.011	6.584	15.081	36.523	75.958	156.32					
\dot{D} (Gy/s)	0	Lx/Tx	1.073	1.033	1.039	1.016	1.019	1.013	1.003	1.005					
T (°C)	15	t (ks)	0.353	1.216	2.943	6.509	15.150	36.606	76.057	152.83					
\dot{D} (Gy/s)	0	Lx/Tx	1.040	1.026	1.029	1.019	0.987	1.004	0.988	0.960					
T (°C)	15	t (ks)	0.353	1.213	2.931	6.478	15.078	36.520	75.955	156.31					
\dot{D} (Gy/s)	0	Lx/Tx	1.032	1.010	0.991	1.000	0.973	0.984	0.932	0.986					

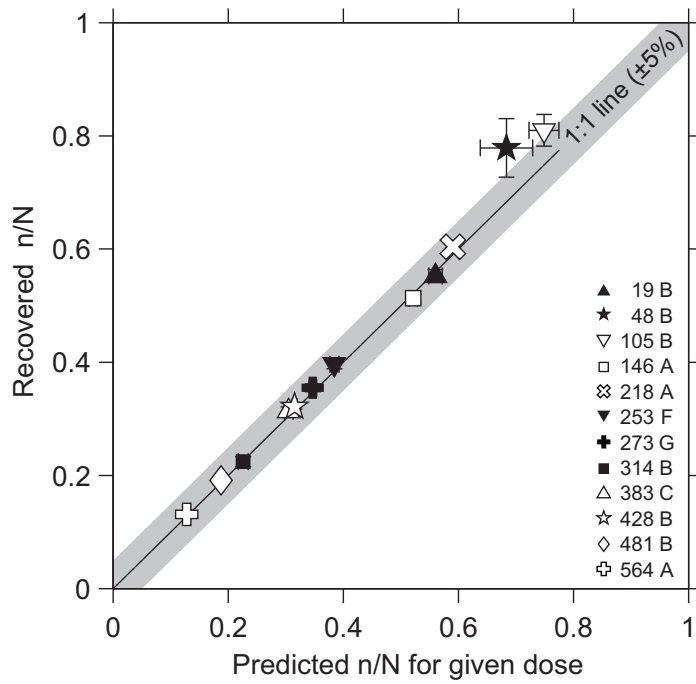


Figure S7. Validation of the dosimetric protocol. Successful recovery of known doses by the SAR protocol is visualized by the 1:1 relationship between predicted (horizontal axis) and recovered (vertical axis) trapped electron concentrations (n/N).

Table S7. Validation of the dosimetric protocol.

Sample		Measurements		Model
Depth (km)	ID	Given dose (Gy)	Recovered n/N	Predicted n/N
0.146	19B	200 ± 10	0.56 ± 0.01	0.55 ± 0.01
0.334	48B	130 ± 7	0.69 ± 0.05	0.79 ± 0.06
0.566	105B	400 ± 20	0.75 ± 0.02	0.81 ± 0.02
0.726	146A	300 ± 15	0.52 ± 0.01	0.51 ± 0.01
0.911	218A	300 ± 15	0.59 ± 0.01	0.60 ± 0.01
1.175	253F	150 ± 8	0.39 ± 0.01	0.40 ± 0.01
1.300	273G	100 ± 5	0.35 ± 0.01	0.35 ± 0.01
1.499	314B	75 ± 4	0.23 ± 0.01	0.22 ± 0.01
1.730	383C	90 ± 5	0.30 ± 0.01	0.31 ± 0.01
1.892	428B	100 ± 5	0.31 ± 0.01	0.32 ± 0.01
2.097	481B	50 ± 3	0.19 ± 0.01	0.19 ± 0.01
2.329	564A	35 ± 2	0.13 ± 0.01	0.13 ± 0.01

Given doses were within 30% of the natural dose of each sample. The average ratio between recovered and predicted trap filling ratios (n/N) is 0.97 ± 0.04 .

Part III – Interpretation

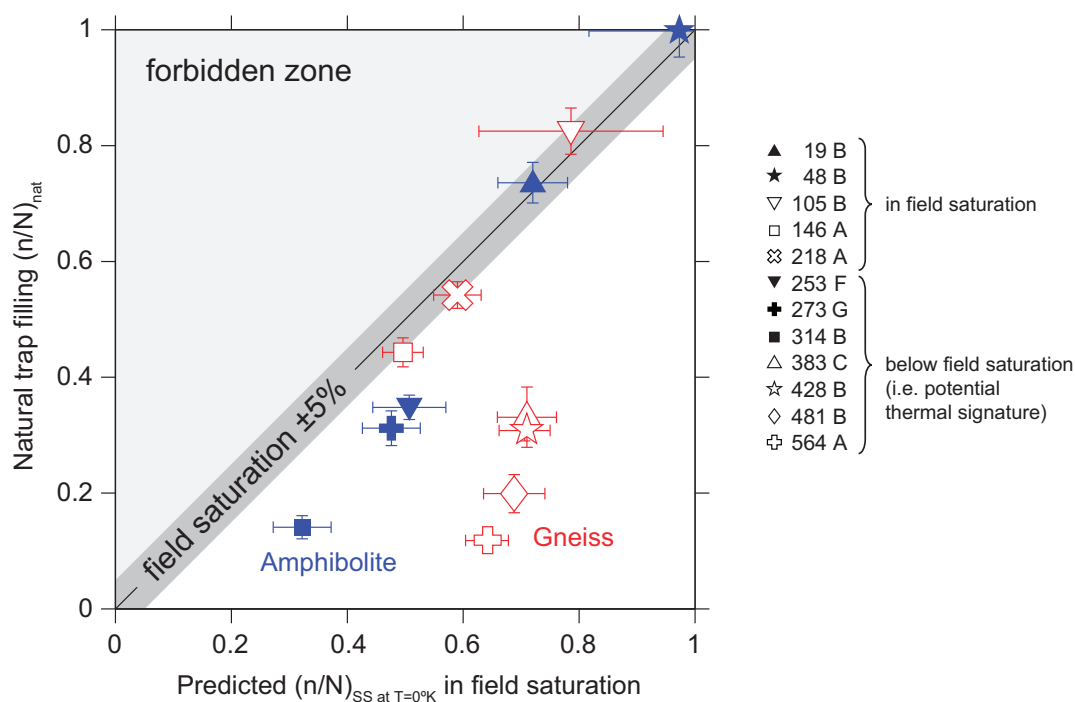


Figure S8. Screening of field-saturated samples. Extending the approach of Kars et al. (2008) to predict trap filling levels in an athermal field steady-state (i.e. mutually-balancing general order trapping and athermal losses; Eqs. 1-2 with $E \rightarrow \infty$ in the main text), we find that the top five KTB samples are in field-saturation in respect to their environmental dose rate and athermal fading, while the bottom seven samples from the borehole are not. Note, that no lithological control over field saturation is observed.

Table S8. Screening of field-saturated samples.

Measurements			Model							Interpretation
Sample	ID	Natural signal (n/N) _{nat}	Predicted field saturation (n/N) _{SS at T=0°K} as a function of dose rate							Natural signal is...
Depth (km)			\bar{D}	\bar{D}_1	\bar{D}_2	\bar{D}_3	\bar{D}_4	$3\bar{D}$	$\bar{D}/3$	
0.146	19B	0.74 ± 0.03	0.72 ± 0.06	0.73	0.74	0.73	0.73	0.74	0.72	in field saturation
0.334	28B	1.00 ± 0.04	0.97 ± 0.16	1.00	1.00	1.00	1.00	1.00	1.00	in field saturation
0.566	105B	0.83 ± 0.04	0.79 ± 0.16	0.83	0.83	0.83	0.83	0.84	0.82	in field saturation
0.726	146A	0.44 ± 0.02	0.50 ± 0.04	0.50	0.50	0.50	0.50	0.52	0.48	in field saturation
0.911	218A	0.54 ± 0.02	0.59 ± 0.04	0.59	0.59	0.59	0.60	0.61	0.58	in field saturation
1.175	253F	0.35 ± 0.02	0.51 ± 0.06	0.51	0.51	0.51	0.51	0.53	0.50	below field saturation
1.300	273G	0.31 ± 0.03	0.48 ± 0.05	0.48	0.47	0.48	0.48	0.50	0.46	below field saturation
1.499	314B	0.14 ± 0.02	0.32 ± 0.05	0.33	0.32	0.33	0.33	0.35	0.31	below field saturation
1.730	383C	0.33 ± 0.05	0.71 ± 0.05	0.72	0.72	0.72	0.72	0.73	0.70	below field saturation
1.892	428B	0.31 ± 0.02	0.71 ± 0.04	0.71	0.70	0.71	0.71	0.72	0.69	below field saturation
2.097	481B	0.20 ± 0.03	0.69 ± 0.05	0.69	0.69	0.69	0.69	0.70	0.68	below field saturation
2.329	564A	0.12 ± 0.01	0.64 ± 0.04	0.65	0.64	0.65	0.65	0.66	0.63	below field saturation

Dose rate scenarios \bar{D}_1 through \bar{D}_4 , and their arithmetic average \bar{D} , are introduced in Supplementary Figure and Table S5. Here, two additional scenarios involving a threefold higher ($3\bar{D}$) and a threefold lower ($\bar{D}/3$) dose rates (relative to \bar{D}) are further used to demonstrate, that across approximately one order of magnitude of environmental radioactivity, the predicted field saturation of the IRS_{L50} electron traps remains essentially the same. Values in bold are further compared against the observed trap filling levels in Supplementary Figure S8.

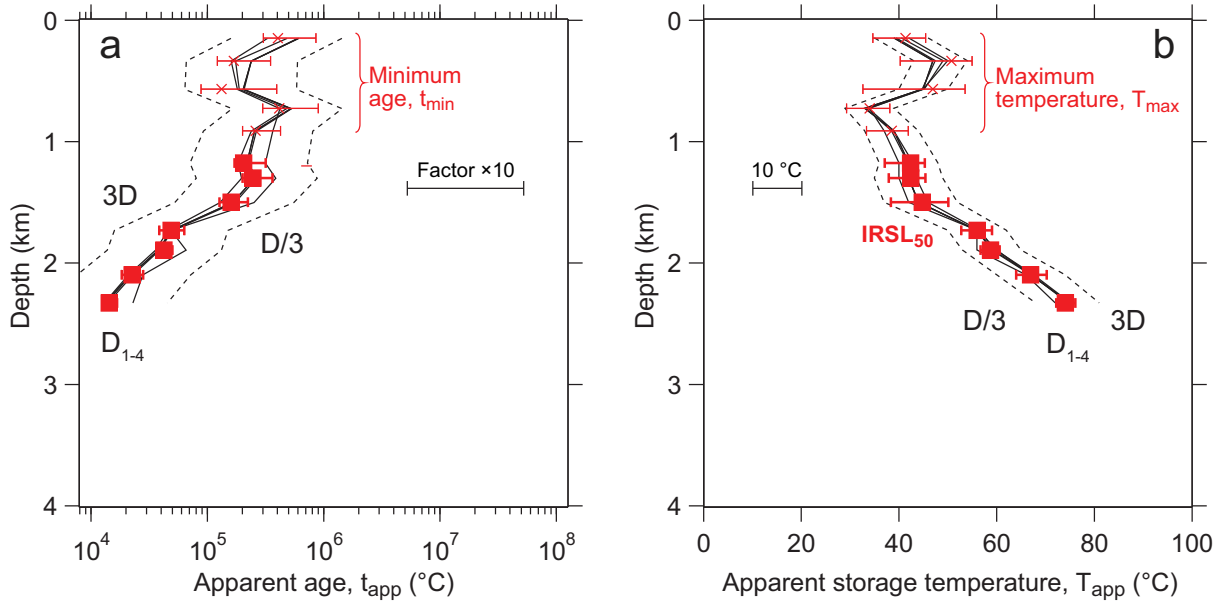


Figure S9. Sensitivity of t_{app} and T_{app} to natural dose rate. (a) Apparent and limiting ages (t_{app} and t_{min}) as calculated for the average-scenario dose rate \dot{D} (red squares and crosses; repeating data from Fig. 4a in the main text), and for alternative dose rate scenarios (lines). Note that a threefold increase ($3\dot{D}$) or decrease ($\dot{D}/3$) in dose rate (dashed lines) leads to a tenfold variation in ages. (b) Apparent and limiting temperatures (T_{app} and T_{max}) as calculated for the average-scenario dose rate \dot{D} (red squares and crosses; repeating data from Fig. 4b in the main text), and for alternative dose rates (lines). Note that T_{app} obtained for a threefold increase or decrease in dose rate (dashed lines) remain well within <10 °C of the average-scenario dose rate.

Table S9. Sensitivity of the inversion to natural dose rate.

Sample		Apparent or limiting age, t_{app} or t_{min} (ka) as a function of dose rate							Apparent or limiting storage temperature T_{app} or T_{max} (°C) as a function of dose rate						
Depth (km)	ID	\dot{D}	\dot{D}_1	\dot{D}_2	\dot{D}_3	\dot{D}_4	$3\dot{D}$	$\dot{D}/3$	\dot{D}	\dot{D}_1	\dot{D}_2	\dot{D}_3	\dot{D}_4	$3\dot{D}$	$\dot{D}/3$
0.146	19B	>403 ⁺⁴⁵⁶ ₋₁₀₀	>602	>331	>613	>487	>160	>1443	<41 ⁺⁴ ₋₇	<39	<42	<39	<40	<46	<35
0.334	28B	>169 ⁺¹⁸¹ ₋₄₇	>240	>161	>240	>176	>66	>600	<51 ⁺⁴ ₋₁₀	<47	<50	<47	<49	<54	<43
0.566	105B	>133 ⁺²⁶² ₋₄₅	>208	>181	>204	>189	>65	>588	<47 ⁺⁷ ₋₁₄	<45	<45	<45	<45	<50	<40
0.726	146A	>415 ⁺⁴⁸⁵ ₋₁₁₅	>532	>423	>524	>482	>164	>1456	<34 ⁺⁴ ₋₅	<33	<34	<33	<34	<39	<29
0.911	218A	>260 ⁺¹⁶⁶ ₋₅₇	>264	>367	>256	>240	>93	>811	<39 ⁺³ ₋₅	<39	<37	<39	<39	<44	<33
1.175	253F	205 ⁺¹¹² ₋₃₄	226	317	220	185	71	729	42 ⁺³ ₋₅	42	40	42	43	48	36
1.300	273G	247 ⁺¹¹⁷ ₋₄₆	266	390	255	198	81	887	42 ⁺³ ₋₅	42	40	42	44	49	35
1.499	314B	160 ⁺⁶³ ₋₃₃	174	253	166	129	53	557	45 ⁺⁵ ₋₆	44	42	44	46	52	37
1.730	383C	49 ⁺¹⁴ ₋₁₀	50	49	49	46	16	151	56 ⁺³ ₋₃	56	56	56	56	62	50
1.892	428B	42 ⁺⁸ ₋₆	39	66	38	36	14	133	59 ⁺² ₋₂	59	56	60	60	65	53
2.097	481B	23 ⁺⁵ ₋₄	23	28	22	21	8	72	67 ⁺³ ₋₃	67	66	67	68	74	60
2.329	564A	14 ⁺² ₋₂	14	23	13	13	5	45	74 ⁺² ₋₂	75	72	75	75	81	68

Dose rate scenarios \dot{D}_1 through \dot{D}_4 , and their arithmetic average \dot{D} , are introduced in Supplementary Figure and Table S5. As in Supplementary Figure and Table S8, here we also use two additional scenarios involving a threefold higher ($3\dot{D}$) and lower ($\dot{D}/3$) dose rates, to demonstrate that while apparent ages are strongly (linearly) dependent on the dose rate, its effect on apparent storage temperatures is weak (logarithmic). Values in bold are apparent/limiting ages and temperatures as reported in Table 4 in the main text.

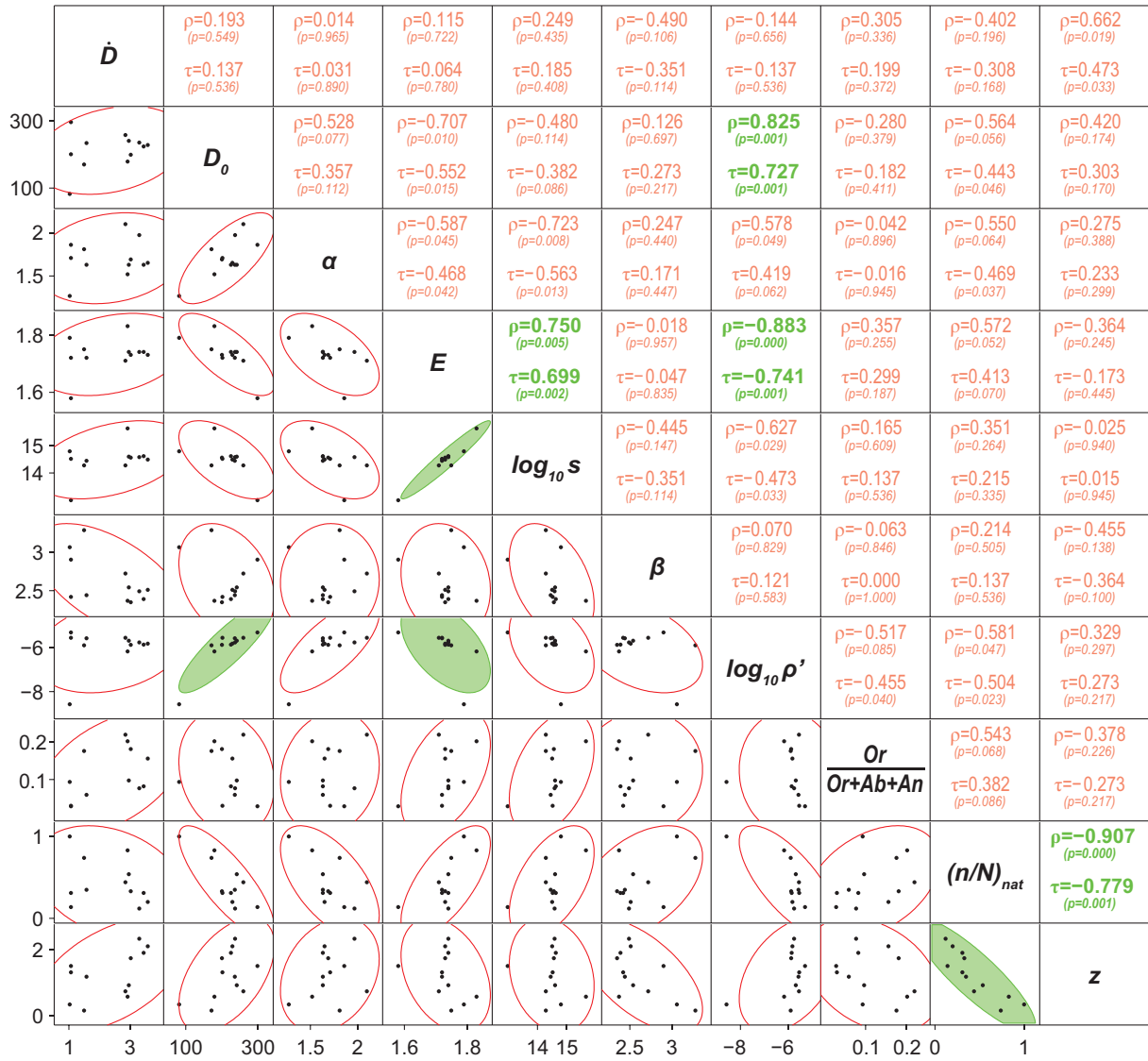


Figure and Table S10. Multivariate statistics on model parameters and observations. Non-parametric rank correlation coefficients due to Spearman (ρ) and Kendall (τ), and the probabilities to obtain lower coefficients (p -values, below). The strongest correlation is observed between natural electron trap filling $(n/N)_{nat}$ and sample depth (z), with $\rho=-0.907$ and $\tau=-0.779$. Four of the strongest correlations (corresponding to the top 10%-percentile) are marked in green; the probability of these correlations being statistically insignificant is $<1\%$. Due to the small sample size (12 observations), we discard all other correlations (whose probability of being insignificant exceeds 1%) as statistically unsupported, pending further proof. Most strikingly, no correlation is observed between depth and any of the kinetic parameters; this strengthens the use of feldspar luminescence for transient cooling conditions, where geological samples move from hot depths towards a colder surface.